Circulating T cell profiles associate with enterotype signatures underlying hematological malignancy relapses

Nicolas Vallet, Maud Salmona, Jeanne Malet-Villemagne, Maxime Bredel, Louise Bondeelle, Simon Tournier, Séverine Mercier-Delarue, Stéphane Cassonnet, Brian Ingram, Régis Peffault de Latour, et al.

Clinical and Translational Report

Cell Host & Microbe

Circulating T cell profiles associate with enterotype signatures underlying hematological malignancy relapses

Graphical abstract

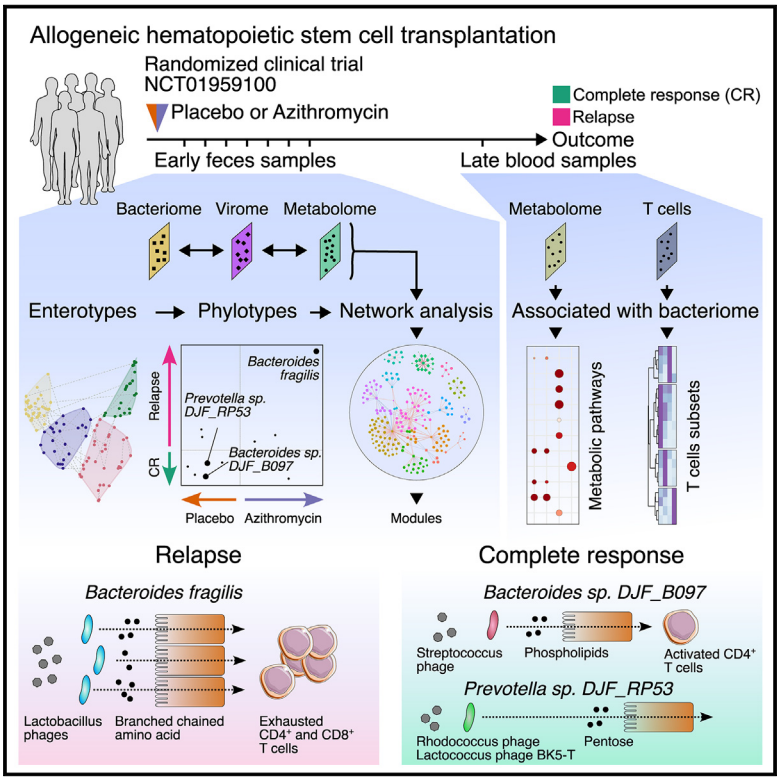

Highlights

- Four enterotypes and their related metabolomes categorize patients after allo-HSCT
- Enterotypes are associated with azithromycin exposure and malignancy relapses
- Networks of bacterial taxa, metabolites, and bacteriophages characterize relapse
- Taxa related to *Bacteroides fragilis* correlate with circulating exhausted T cells

Authors

Nicolas Vallet, Maud Salmona, Jeanne Malet-Villemagne, ..., Jérome Le Goff, Patricia Lepage, David Michonneau

Correspondence

david.michonneau@aphp.fr

In brief

Exposure to azithromycin after allogeneic hematopoietic stem cell transplantation increases the relapse rate of hematological malignancies. Michonneau and colleagues reveal specific networks of gut bacteria, metabolites, and bacteriophages associated with azithromycin intake and hematologic relapse. Enterotypes and taxa correlate with plasma metabolome and with functional profiles of circulating immune cells.

Vallet et al., 2023, Cell Host & Microbe *31*, 1386–1403
August 9, 2023
https://doi.org/10.1016/j.chom.2023.06.009

CellPress

CellPress

Cell Host & Microbe

Clinical and Translational Report

Circulating T cell profiles associate with enterotype signatures underlying hematological malignancy relapses

Nicolas Vallet,[1] Maud Salmona,[1,2] Jeanne Malet-Villemagne,[3] Maxime Bredel,[3] Louise Bondeelle,[4] Simon Tournier,[5] Séverine Mercier-Delarue,[2] Stéphane Cassonnet,[6] Brian Ingram,[7] Régis Peffault de Latour,[8,9] Anne Bergeron,[10] Gérard Socié,[1,8] Jérome Le Goff,[1,2,11] Patricia Lepage,[3,11] and David Michonneau[1,8,11,12,*]

[1]Université de Paris Cité, INSERM U976, 75010 Paris, France
[2]Virology Department, AP-HP, Saint-Louis Hospital, 75010 Paris, France
[3]Université Paris-Saclay, INRAE, AgroParisTech, Micalis Institute, Domaine de Vilvert, 78350 Jouy-en-Josas, France
[4]Pneumology Unit, AP-HP, Saint-Louis Hospital, 75010 Paris, France
[5]Core Facilities, Saint-Louis Research Institute, Université de Paris Cité, UAR 2030/US 53, 75010 Paris, France
[6]Service de Biostatistique et Information Médicale, AP-HP, Saint-Louis Hospital, 75010 Paris, France
[7]Metabolon, Inc., Morrisville, NC 27560, USA
[8]Hematology Transplantation, AP-HP, Saint-Louis Hospital, 1 avenue Claude Vellefaux, 75010 Paris, France
[9]Cryostem Consortium, 13382 Marseille, France
[10]Pneumology Department, Geneva University Hospitals, 1205 Geneva, Switzerland
[11]Senior author
[12]Lead contact
*Correspondence: david.michonneau@aphp.fr
https://doi.org/10.1016/j.chom.2023.06.009

SUMMARY

Early administration of azithromycin after allogeneic hematopoietic stem cell transplantation was shown to increase the relapse of hematological malignancies. To determine the impact of azithromycin on the post-transplant gut ecosystem and its influence on relapse, we characterized overtime gut bacteriome, virome, and metabolome of 55 patients treated with azithromycin or a placebo. We describe four enterotypes and the network of associated bacteriophage species and metabolic pathways. One enterotype associates with sustained remission. One taxon from *Bacteroides* specifically associates with relapse, while two from *Bacteroides* and *Prevotella* correlate with complete remission. These taxa are associated with lipid, pentose, and branched-chain amino acid metabolic pathways and several bacteriophage species. Enterotypes and taxa associate with exhausted T cells and the functional status of circulating immune cells. These results illustrate how an antibiotic influences a complex network of gut bacteria, viruses, and metabolites and may promote cancer relapse through modifications of immune cells.

INTRODUCTION

Allogeneic hematopoietic stem cell transplantation (allo-HSCT) is a curative treatment of hematological malignancies.[1] Despite improvements in prophylactic and pre-emptive treatments, relapse remains the main cause of death following allo-HSCT.[2] The curative graft-versus-tumor (GVT) effect relies on the alloreactivity of donor immune cells against tumor cells.[3] GVT is mainly mediated by donor T cells, as illustrated by the higher risk of relapse associated with T cell-depleted grafts[4] and the preventive effects of donor lymphocyte infusions (DLIs).[5] However, allo-HSCT benefits are counterbalanced by graft-versus-host disease (GVHD), in which T cells target host healthy tissues.[4,6,7] Understanding the specificities of tumor- and healthy-tissue-directed alloreactivity is crucial to develop strategies that enhance GVT without increasing GVHD.

Lung chronic GVHD (cGVHD), clinically recognized as bronchiolitis obliterans syndrome (BOS), occurs in 10% of patients mainly in the first 2 years after HSCT[8] and shares physiopathological mechanisms with BOS[9] that occur after lung transplantation. After lung transplantation, azithromycin, a second-generation macrolide, can prevent BOS.[10] These observations led us to evaluate azithromycin as a lung cGVHD prophylaxis in a randomized, multi-center, placebo-controlled, double-blind, superiority study (ALLOZITHRO trial, NCT01959100). Unexpectedly, azithromycin was associated with a higher risk of relapse (hazard ratio [HR] = 1.7) and increased death rate, while it did not prevent acute GVHD or cGVHD.[11] This led to both the Food and Drug Administration and the European Medicines Agency warning about azithromycin use early after allo-HSCT.[12]

Gut microbiota are disturbed after allo-HSCT.[13] This dysbiosis is characterized by lower alpha diversity and *Enterococcus*

domination.[14,15] Antibiotics used during and before the procedure influence the abundance of bacterial species and bacterial domination.[16–18] Parenteral nutrition also influences gut microbiota composition.[19] Lower microbial diversity has been associated with a higher risk of non-relapse mortality.[15,20] Few studies report the link between gut microbiota and allo-HSCT relapse. Low frequency of *Blautia* genus has been associated with a higher risk of relapse[19] and a cluster of phylotypes (operational taxonomic units [OTUs]), mainly comprising *Eubacterium limosum*, was associated with a lower risk of relapse.[21] However, mechanisms underlying the role of gut microbiota in antitumor responses after allo-HSCT are still unknown; however, they might be related to gut-microbiome-derived metabolites.[22,23] Additionally, we previously reported that the gut eukaryotic virome is associated with enteric GVHD after allo-HSCT.[24] Although gut microbiota and metabolites are influenced by bacteriophages,[25,26] their reciprocal impact and associations following allo-HSCT is ill-defined.[27]

We recently highlighted an off-target effect of azithromycin, which impairs the antitumor immune response by directly affecting the metabolism of T cell energy and T cell receptor (TCR) signaling.[28] Considering the expected on-target effects of azithromycin on gut microbiota and its role in allo-HSCT outcome, we hypothesized that azithromycin may promote relapse after allo-HSCT through its impact on the gut ecosystem.

To decipher how gut bacteriome, virome, and metabolomic profiles interact over time during the allo-HSCT procedure, we applied a multi-omic approach on fecal samples from patients included in the ALLOZITHRO trial. We first characterized gut microbiome and described four bacterial enterotypes and their connections with metabolites and viral species. Enterotypes and their associated viruses and metabolic pathways were independently associated with azithromycin or a placebo intake and with relapse or remission. Then, focusing on azithromycin- and relapse-associated microbial taxa, we highlighted a network of bacteria, bacteriophages, and metabolic pathways associated with post-transplant relapses and azithromycin intake. Ultimately, we uncovered peripheral blood T cell exhaustion profiles associated with enterotypes and with relapse-associated bacterial taxa.

RESULTS

Cohort

Fecal samples from patients included in the ALLOZITHRO trial were collected over time, including 27 patients from the azithromycin arm (n = 73 samples) and 28 patients from the placebo arm (n = 75 samples). The first and last samples were collected from the week before allo-HSCT and 6 weeks after allo-HSCT, respectively (Figure 1A). Most samples were assessed for all omics (n = 92), including 43 and 49 in the placebo and azithromycin cohorts, respectively (Figure 1B). Characteristics of patients included in the placebo and azithromycin cohorts were similar (Table S1). Higher risk of relapse in patients included in the azithromycin arm was consistent with ALLOZITHRO trial (HR = 1.65, 95% confidence interval [95% CI]: 0.68–4.00, Figures S1A and S1B). Nutrition support and concomitant antibiotics used were also similar in both arms and detailed in Table S2.

Post-transplant gut microbiota stratified samples into four enterotypes

As previously described,[15,17] bacterial alpha diversity decreased during the procedure, mainly during the first 2 weeks after transplantation (Figure S1C). We uncovered four clusters of samples (Figure 2A), i.e., enterotypes. These clusters were associated with alpha diversity: cluster 2 exhibited the highest diversity, followed by cluster 1, 3, and 4 (Figure 2B). Enterotype 1 was characterized by *Clostridium XIVa* and *Parabacteroides* genera. Enterotype 2 was characterized by *Bacteroides*, *Fusobacterium*, and *Faecalibacterium*. Higher relative abundances of *Bacteroides* were found in enterotype 3, while enterotype 4 was driven by *Enterococcus* and *Enterobacter* genera (Figure 2C). Both enterotypes 2 and 3 were enriched in *Bacteroides* genus. However, microbial richness and diversity were both significantly lower in enterotype 3 (Figure 2B). Compared with enterotype 2, enterotype 3 was predominantly enriched in *Bacteroides vulgatus* and *Bacteroides fragilis*, while enterotype 2 was enriched in *Bacteroides uniformis*, *Bacteroides sp. Smarlab BioMol-2301151*, *Bacteroides ovatus*, and *Bacteroides massiliensis* (Figures S2A–S2C).

Enterotypes are associated with azithromycin treatment and subsequent relapse

We first evaluated whether enterotypes were associated with azithromycin or a placebo intake and relapse or complete remission at 12 months.

The treatment (azithromycin or a placebo) was significantly associated with enterotypes ($p = 0.037$). Enterotypes 3 and 4 were equally distributed in azithromycin and placebo samples, enterotype 1 (driven by *Clostridium XIVa* and *Parabacteroides*) was associated with 70% of samples from the azithromycin group (n = 23), while 68% of samples from the placebo group belonged to enterotype 2 (driven by *Bacteroides*, *Fusobacterium*, and *Faecalibacterium*; n = 17, $p = 0.02$) (Figure 3A).

Post-transplantation relapse of the underlying malignant disease at 12 months was also associated with enterotypes distribution ($p = 0.026$). Enterotype 2 was mainly associated with complete remission (95.5%), while enterotypes 1, 3, and 4 were associated with 10 (32%, $p = 0.017$); 12 (38%, $p = 0.008$); and 10 (42%, $p = 0.005$) samples from relapsing patients, respectively (Figure 3B).

We did not observe any association or pattern between enterotypes and time (Figures S3A–S3E). We also integrated time-to-sample collection in association with azithromycin or placebo and relapse or complete responses, as illustrated in Figure S3F. This figure highlights the frequency of outcome within each enterotype at a given time point. It shows that enterotype 2 is strongly associated with placebo intake and complete response, independently from the time elapsed post transplantation. In addition, compared with those with stable enterotypes, patients who changed enterotypes during the transplantation procedure were associated with less relapse (complete remission at 12 months, 77% versus 38%, $p = 0.020$). Shift in enterotype was not influenced by clinical variables or by the type of antibiotics used (Table S3).

Hematological status (complete response or relapse) and treatment arm (placebo or azithromycin) were still associated with enterotypes in multivariate multinomial regression models that also included confounding variables associated with

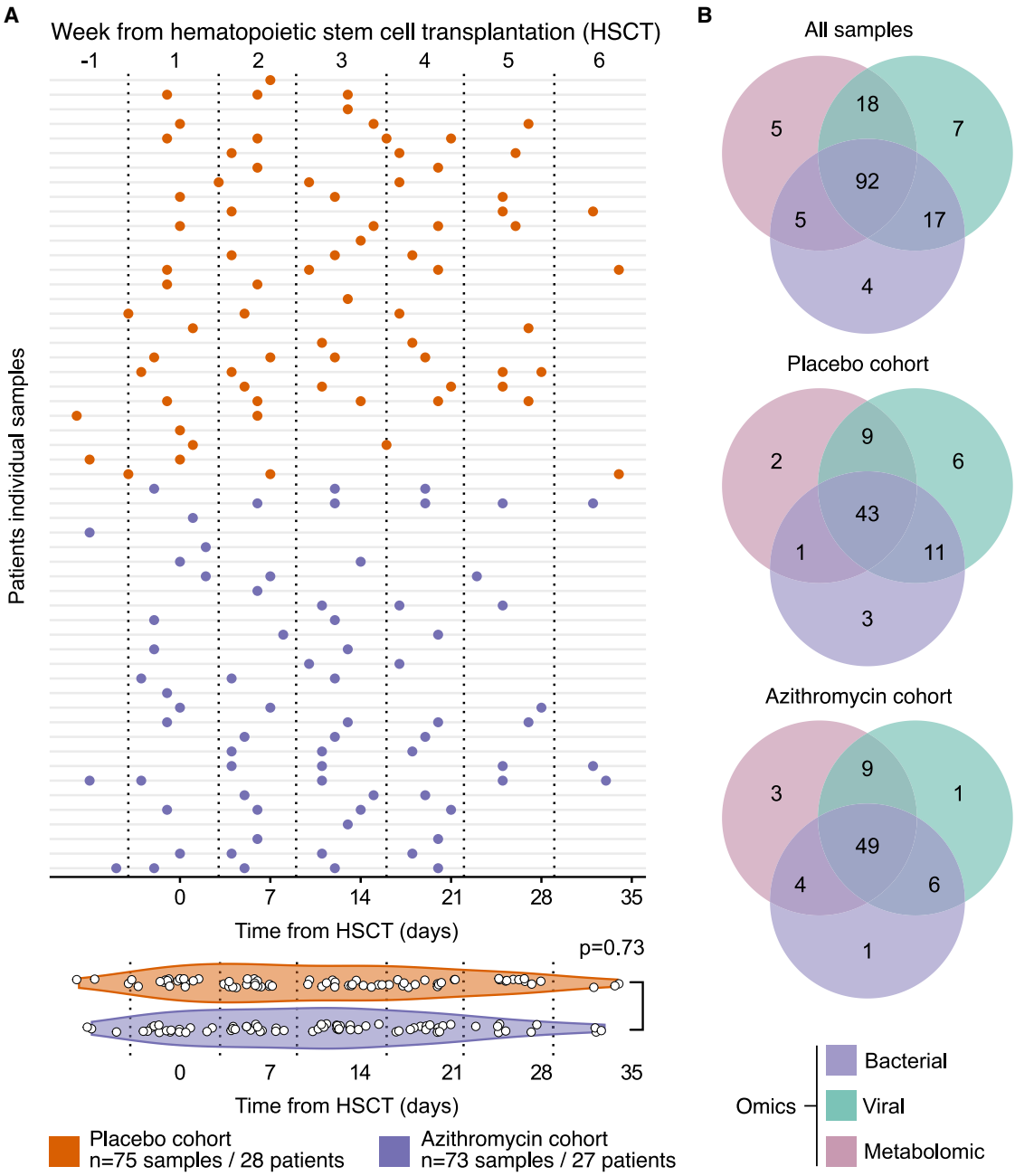

Figure 1. Overview of the studied samples

(A) Distribution of the samples according to the time elapsed from allogeneic hematopoietic stem cell transplantation (HSCT) and azithromycin or placebo cohorts. One dot represents one sample from one patient (either from one or three omics). A non-parametric, bilateral Wilcoxon test was performed to compare the time elapsed from HSCT.

(B) Venn diagrams depicting the distribution of omics data available from all samples studied, those from the placebo cohort and the azithromycin cohort.

See also Figure S1 and Tables S1 and S2.

enterotypes (disease risk index, type of donor, source of stem cells, and GVHD prophylaxis) (Table 1; Figure S4A).

Considering co-medication with other anti-infectious treatments, enterotypes were associated with amoxicillin ($p = 0.002$), piperacillin-tazobactam ($p < 0.001$), imipenem/cilastatin ($p = 0.002$), ganciclovir ($p = 0.036$), and caspofungin ($p = 0.020$) (Table 1). Because antibiotic combinations may be used during the procedure, we studied the distribution of antimicrobial intake in a multivariate analysis using correspondence analysis. This revealed that compared with other enterotypes, (1) enterotype 4 was mainly associated with metronidazole and cefotaxime treatments; (2) enterotype 1 was associated with imipenem/cilastatin, ganciclovir, azithromycin, posaconazole, and ceftriaxone; (3) enterotype 3 with levofloxacin and ceftriaxone; and (4) enterotype 2

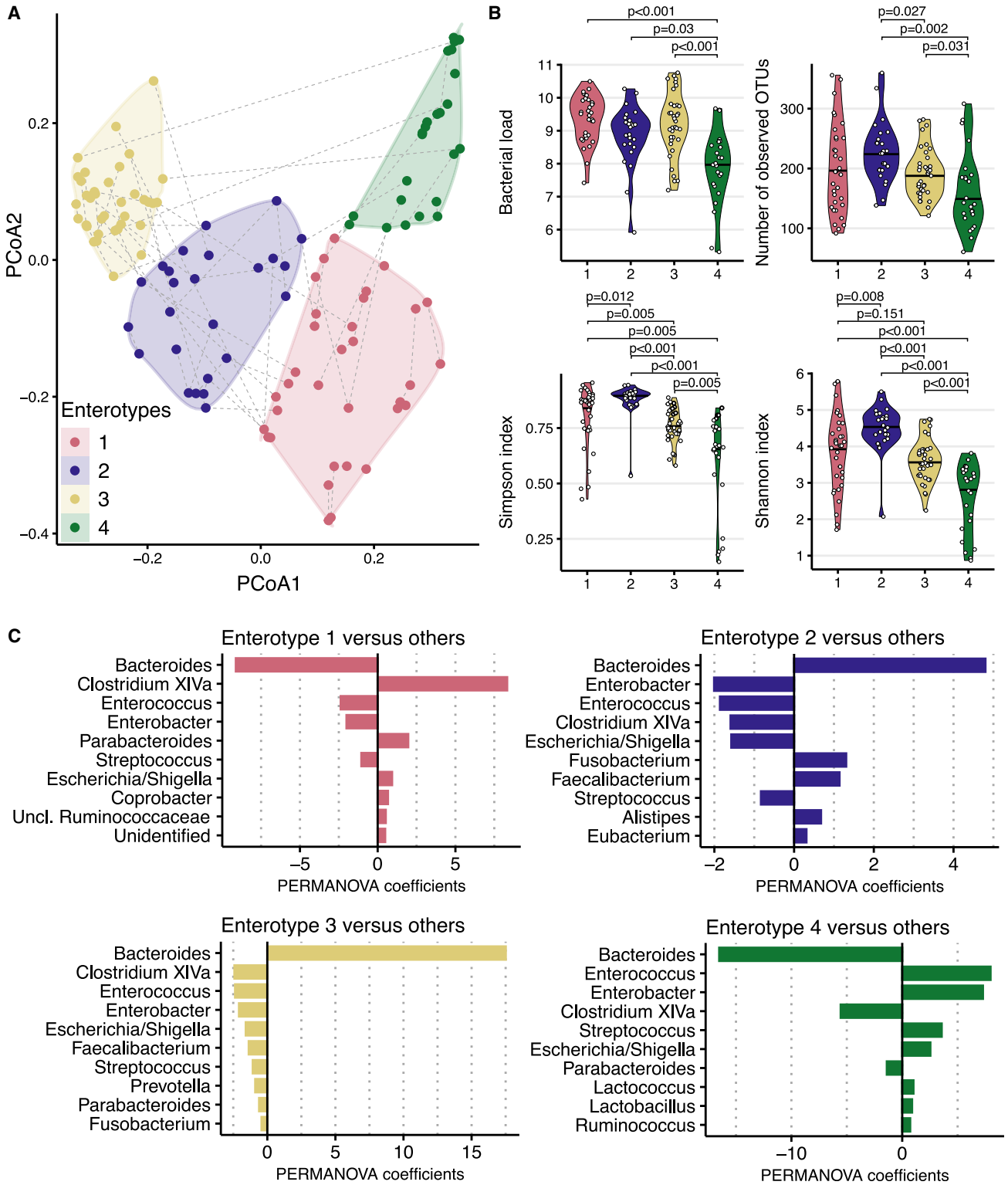

Figure 2. Post-transplant gut microbiota enterotypes

(A) Dot plot depicting co-ordinates of each sample on the first and second axes of principal co-ordinate analysis (PCoA) performed from a Bray-Curtis matrix distance. Samples were clustered with hierarchical k-means. Each cluster defines an enterotype. Dotted gray line links samples from a same patient.

(B) Violin plots of alpha-diversity indexes according to diverse enterotypes. p values were computed with non-parametric bilateral Wilcoxon test.

(C) Bar plots exhibiting top genera permutational multivariate analysis of variance (PERMANOVA) co-efficient in each enterotype.

See also Figure S2 and Table S3.

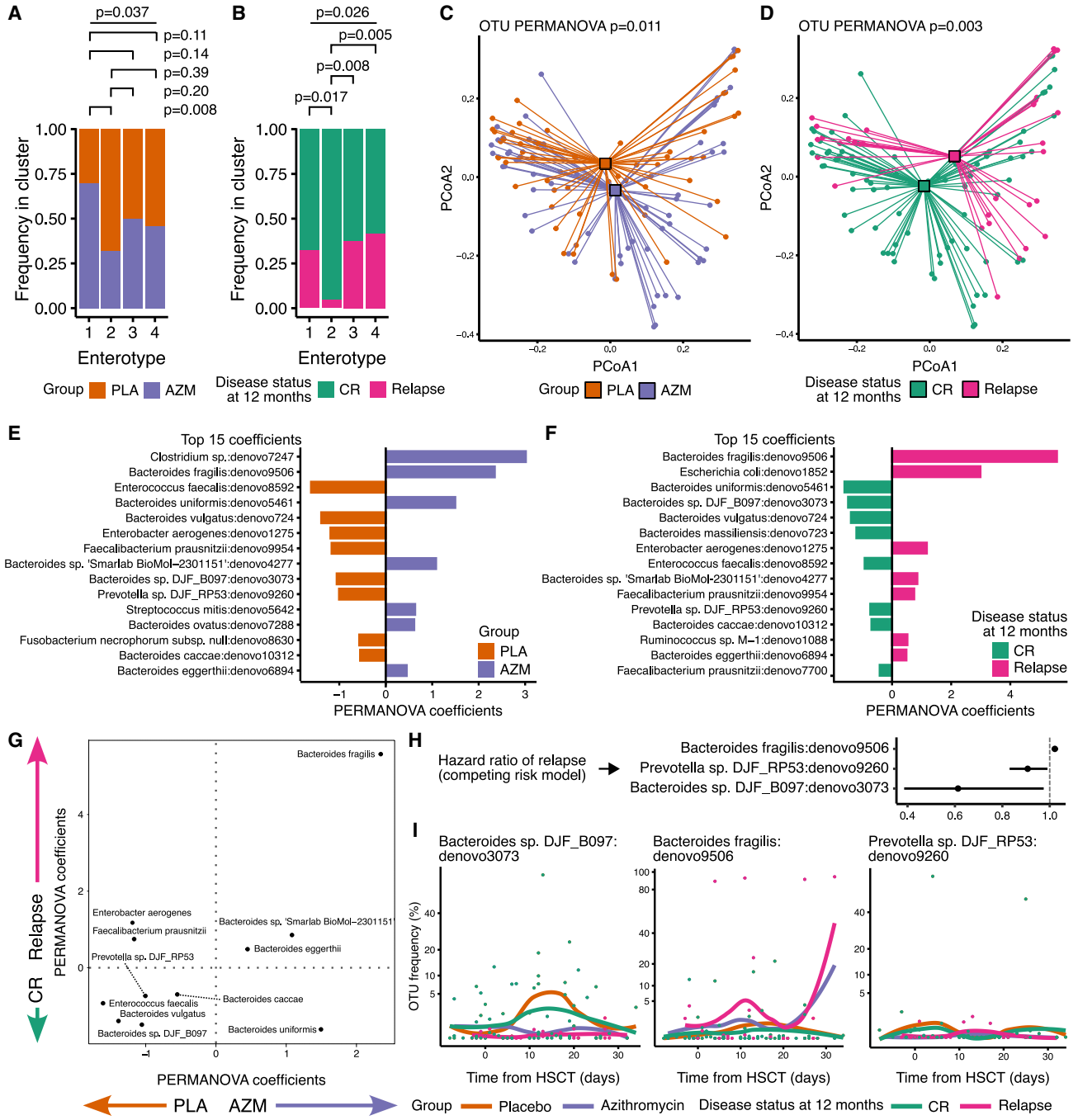

Figure 3. Specific gut microbiota associated with azithromycin intake and relapse after transplantation

(A and B) Bar plot showing the frequencies of samples in the group of randomization and complete remission at 12 months according to enterotypes. P values were computed with the non-parametric bilateral Wilcoxon test.

(C and D) Dot plot depicting principal co-ordinate analysis (PCoA) computed from Bray-Curtis distance matrix. Squares show barycenter of each group.

(E and F) Bar plots represent top 15 phylotypes that drive the differences between the groups (PERMANOVA coefficients). (C) Comparing patients from the azithromycin arm with those from the placebo arm. (F) Comparing patients in relapse at 12 months and those in complete remission.

(G) Dot plot showing PERMANOVA coefficients of phylotype found in the top 15 coefficients in both relapse/complete remission and azithromycin/placebo enterotypes.

(H) Forest plot showing hazard ratio and 95% confidence intervals of relapse according to Fine and Gray competing risk model of relapse, with death not related to relapse as a competing risk. The analysis was performed with phylotypes shown in (C) after computing mean OTU abundances for each patient. For visualization purposes, only significant phylotypes are shown.

(legend continued on next page)

was not associated with a specific antimicrobial compared with the others (Figure S4B).

Together, these results highlight that among antimicrobials, azithromycin was associated with higher frequency of enterotype 1 driven by *Clostridium XlVa* and *Parabacteroides* genera, while placebo intake and complete remission were associated with higher frequency of enterotype 2 driven by *Bacteroides*, *Fusobacterium*, and *Faecalibacterium*.

Azithromycin treatment and hematological malignancy relapse share gut microbiota taxa

To unravel the microbial specificity associated with azithromycin or a placebo intake and with relapse or complete remission, we directly compared the samples using permutational multivariate analysis of variance (PERMANOVA). Azithromycin-associated microbiota were significantly different from placebo-associated microbiota ($p = 0.011$) (Figure 3C). Relapse and complete remission were also statistically different ($p = 0.003$) (Figure 3D).

To gain insights on potential differences in bacterial species, we studied phylotypes that drove these differences. Among the top driving phylotypes, those related to *Clostridium sp*, *B. fragilis*, *B. uniformis*, and *Bacteroides sp. Smarlab Biomol-2301151* were associated with azithromycin, while *E. faecalis*, *B. vulgatus*, *E. aerogenes*, *F. prausnitzii*, *Bacteroides sp. DJF_B097*, and *Prevotella sp. DJF_RP53* were associated with a placebo (Figure 3E). Likewise, complete remission and relapses were associated with specific microbiota (PERMANOVA $p = 0.003$). Relapse-associated microbiota were mainly characterized by phylotypes related to *B. fragilis*, *E. coli*, and *E. aerogenes*, whereas remission was associated with relatives of *B. uniformis*, *Bacteroides sp. DJF_B097*, *B. vulgatus*, *B. massiliensis*, and *E. faecalis* (Figure 3F).

Consistent with the higher risk of relapse in the azithromycin group in the ALLOZITHRO trial, among the common driving phylotypes, 10/13 (77%) were associated with relapse and azithromycin or with placebo and complete remission (Figure 3G). Among these 10 phylotypes, those relatives of *B. fragilis*, *Bacteroides sp. Smarlab BioMol-2301151*, and *B. eggerthii* were associated with relapse and azithromycin, whereas *B. vulgatus*, *Bacteroides sp. DJF_B097*, *E. faecalis*, *Prevotella sp. DJF_RP53*, *B. caccae*, *P. oralis*, and *Bacteroides sp. CCUG 39913* were associated with placebo and complete remission (Figure 3G). Time integration to the analysis allowed the identification of a dynamic microbial signature associated with relapse ($p = 0.0003$). Phylotypes related to *B. caccae*, *B. uniformis*, *F. prausnitzii*, *E. faecalis*, *B. sp. CCUG 39913*, and *B. fragilis* drove the signature toward relapse, while *Prevotella sp DJF_RP53*, *E. aerogenes*, *B. vulgatus*, *Bacteroides sp. DJF_B097*, *B. eggerthii*, and *Bacteroides sp. Smarlab BioMol-2301151* were associated with complete response (Figures S4C and S4D).

To determine which phylotypes were associated with relapse, after considering the time-dependent nature of this outcome and death as a competing risk, a Fine and Gray model was computed using mean OTU abundances for each patient. Results revealed that *B. fragilis* taxon was associated with higher risk of relapse (HR = 1.02, 95%CI: 1.02–1.03, $p < 0.001$). Two other phylotypes were associated with lower risk of relapse: *Prevotella sp. DJF_RP53* (HR = 0.90, 95% CI: 0.85–0.94, $p < 0.001$) and *Bacteroides sp. DJF_B097* (HR = 0.69, 95% CI: 0.57–0.82, $p < 0.001$) (Figure 3H).

The frequency of the profiles over time of the three latter phylotypes were comparable between complete remission and placebo or between azithromycin and relapsing patients. The phylotype related to *Bacteroides sp. DJF_B097* was lower in azithromycin and the relapsing patient. *Prevotella sp. DJF_RP53*'s profiles of the relapsed/azithromycin groups inversely correlated with the profile of the complete remission/placebo groups. By contrast, *B. fragilis*' profiles were consistent with higher frequencies in azithromycin and relapsing patients (Figure 3I). None of these phylotypes correlated together, suggesting that their trajectories were independent (Figure S4E).

Altogether, these results show that azithromycin intake impacted *Bacteroides sp. DJF_B097*, *Prevotella sp. DJF_RP53*, and *B. fragilis*, which were also associated with subsequent hematological response.

Deciphering multi-omics modules associated with enterotypes

Gut virome was not specifically associated with azithromycin treatment and relapse (Figure S5). Among the 925 studied metabolites, N-acetyl-cadaverine, pyridoxal, pyridoxamine, and 5-(2-hydroxyethyl)-4-methylthiazole levels were higher in placebo-treated patients than in the azithromycin-treated patients, and none were significantly associated with relapse (Figure S5). These results suggest that gut bacteriome was the main contributor to identify relapse in patients.

To understand how enterotypes may be linked with host metabolism, we next explored the gut metabolome. Ninety-nine metabolites were significantly associated with the distribution of the four enterotypes (Figure 4A). The enrichment analysis revealed that enterotypes were associated with specific metabolic pathways (Figure 4B). All enterotypes, except number 4, were associated with secondary bile acid metabolism. Enterotype 4 exhibited enrichment of primary bile acid and lysophospholipids metabolism. Enterotype 1 was enriched in lysophospholipids and secondary bile acid metabolism. Enterotypes 2 and 3 were close together and characterized by the enrichment of metabolites involved in secondary bile acid metabolism and pyrimidine metabolism (Figure 4B).

To investigate whether gut virome could be associated with gut microbiota composition after allo-HSCT, we studied viral species in fecal samples. Individual viruses were not associated with bacterial enterotypes (Data S1, S2, S3, and S4). Similarly, clusters of viral samples were not associated with enterotypes (Figures 4C, 4D, and S6). Comparison of viral composition and metabolite levels of samples from enterotype 2 with those from

(l) Dot plot and regression line with 95% confidence interval showing frequencies of phylotypes associated with relapse during the first months after allogeneic hematopoietic stem cell transplantation (HSCT).

CR, complete remission; OTUs, operational taxonomic units; AZM, azithromycin; PLA, placebo; PERMANOVA, permutational multivariate analysis of variance. See also Figures S3–S5.

Table 1. Enterotypes clinical characteristics

	Enterotypes				
	1	2	3	4	p value
Number of samples	33	25	36	24	N/A
Gender, female	8 (24%)	6 (24%)	10 (28%)	10 (42%)	0.5
Age (years)	59 (43–62)	57 (49–64)	56 (48–65)	55 (27–62)	0.2
Group					
Placebo	10 (30%)	17 (68%)	18 (50%)	13 (54%)	0.037
Azithromycin	23 (70%)	8 (32%)	18 (50%)	11 (46%)	N/A
Diagnosis					
Acute lymphoid leukemia	9 (27%)	2 (8.0%)	3 (8.3%)	6 (25%)	N/A
Acute myeloid leukemia	6 (18%)	3 (12%)	7 (19%)	7 (29%)	N/A
Chronic lymphoid leukemia	1 (3.0%)	2 (8.0%)	2 (5.6%)	4 (17%)	N/A
Chronic myeloid leukemia	1 (3.0%)	0 (0%)	0 (0%)	0 (0%)	N/A
Hodgkin lymphoma	0 (0%)	0 (0%)	1 (2.8%)	1 (4.2%)	N/A
Myelodysplastic neoplasm	7 (21%)	8 (32%)	7 (19%)	2 (8.3%)	N/A
Non-Hodgkin lymphoma	4 (12%)	7 (28%)	4 (11%)	4 (17%)	N/A
Other malignancies	5 (15%)	3 (12%)	12 (33%)	0 (0%)	N/A
Disease risk index					
Low	0 (0%)	2 (8.0%)	0 (%)	4 (17%)	0.06
Intermediate	9 (27%)	10 (40%)	14 (39%)	8 (33%)	N/A
High	24 (73%)	13 (52%)	22 (61%)	12 (50%)	N/A
Disease status at transplant					
>CR1	12 (36%)	4 (16%)	5 (14%)	7 (29%)	0.4
CR1	9 (27%)	10 (40%)	13 (36%)	7 (29%)	N/A
Other	12 (36%)	11 (44%)	18 (50%)	10 (42%)	N/A
Type of donor					
Related	8 (24%)	8 (32%)	20 (56%)	8 (33%)	0.046
Unrelated	25 (76%)	17 (68%)	16 (44%)	16 (67%)	N/A
Cytomegalovirus (CMV) serology (donor/recipient)					
−/−	9 (27%)	7 (28%)	8 (22%)	11 (46%)	0.17
−/+	11 (33%)	8 (32%)	5 (14%)	2 (8.3%)	N/A
+/−	5 (15%)	2 (8.0%)	8 (22%)	3 (12%)	N/A
+/+	8 (24%)	8 (32%)	15 (42%)	8 (33%)	N/A
Source of stem cells					
Peripheral blood	26 (79%)	24 (96%)	35 (97%)	20 (83%)	0.044
Bone marrow	2 (6.1%)	1 (4.0%)	0 (0%)	3 (12%)	N/A
Cord blood	5 (15%)	0 (0%)	1 (2.8%)	1 (4.2%)	N/A
Conditioning regimen					
Myeloablative	8 (24%)	3 (12%)	9 (25%)	10 (42%)	0.12
Non myeloablative	25 (76%)	22 (88%)	27 (75%)	14 (58%)	N/A
GVHD prophylaxis					
Cyclosporine-MTX	12 (36%)	1 (4.0%)	8 (22%)	7 (29%)	0.038
Cyclosporine-MMF	20 (61%)	21 (84%)	26 (72%)	17 (71%)	N/A
Other	1 (3.0%)	3 (12%)	2 (5.6%)	0 (0%)	N/A
Acute GVHD					
aGVHD	26 (79%)	15 (60%)	19 (53%)	12 (50%)	0.14
Death before aGVHD	5 (15%)	5 (20%)	7 (19%)	8 (33%)	N/A
No event at the last follow-up	2 (6.1%)	5 (20%)	10 (28%)	4 (17%)	N/A

(*Continued on next page*)

Table 1. ***Continued***

	Enterotypes				
	1	2	3	4	p value
Chronic GVHD					
Mild	16 (67%)	11 (85%)	7 (47%)	6 (46%)	0.20
Moderate	7 (29%)	1 (7.7%)	6 (40%)	6 (46%)	N/A
Severe	1 (4.2%)	1 (7.7%)	2 (13%)	1 (7.7%)	N/A
No event at the last follow-up	9	12	21	11	N/A
Bronchiolitis obliterans syndrome					
Yes	0	0	1	1	N/A
Relapse at 12 months					
No event at 12 months	21 (68%)	21 (95%)	20 (62%)	14 (58%)	0.026
Relapse	10 (32%)	1 (4.5%)	12 (38%)	10 (42%)	N/A
Death before 12 months	2	3	4	0	N/A
Nutrition					
Enteral	5 (15%)	3 (12%)	5 (14%)	6 (29%)	0.092
Oral	22 (67%)	18 (72%)	22 (61%)	6 (29%)	N/A
Intravenous	6 (18%)	4 (16%)	9 (25%)	9 (43%)	N/A
Unknown	0	0	0	3	N/A
Beta-lactamin					
Amoxicillin	33 (100%)	25 (100%)	35 (97%)	19 (79%)	0.002
Piperacillin-tazobactam	26 (79%)	18 (72%)	15 (42%)	21 (88%)	<0.001
Glycopeptide					
Vancomycin	12 (36%)	12 (48%)	8 (22%)	11 (46%)	0.14
Cephalosporin					
Ceftriaxone	1 (3.0%)	1 (4.0%)	1 (2.8%)	0 (0%)	>0.9
Cephazolin	8 (24%)	6 (24%)	5 (14%)	10 (42%)	0.11
Ceftazidime	10 (30%)	8 (32%)	5 (14%)	5 (21%)	0.3
Cefoxatime	0 (0%)	0 (0%)	0 (0%)	1 (4.2%)	0.2
Quinolone					
Ofloxacin	33 (100%)	25 (100%)	34 (94%)	23 (96%)	0.4
Levofloxacin	0 (0%)	2 (8.0%)	1 (2.8%)	0 (0%)	0.3
Carbapenem					
Imipenem-cilastatin	11 (33%)	2 (8.0%)	1 (2.8%)	2 (8.3%)	0.002
Sulfonamides					
Sulfamethoxazole-trimethoprim	33 (100%)	25 (100%)	36 (100%)	24 (100%)	N/A
Nitroimidazole					
Metronidazole	0 (0%)	0 (0%)	0 (0%)	1 (4.2%)	0.2
Aminoglycoside					
Amikacin	28 (85%)	22 (88%)	32 (89%)	22 (92%)	>0.9
Anti-viral					
Valaciclovir	33 (100%)	25 (100%)	35 (97%)	23 (96%)	0.7
Ganciclovir	5 (15%)	6 (24%)	1 (2.8%)	1 (4.2%)	0.036
Anti-fungal					
Micafungin	0 (0%)	0 (0%)	0 (0%)	0 (0%)	N/A
Posaconazole	5 (15%)	2 (8.0%)	1 (2.8%)	0 (0%)	0.11
Viroconazole	5 (15%)	6 (24%)	2 (5.6%)	7 (29%)	0.065
Fluconazole	10 (30%)	5 (20%)	11 (31%)	8 (33%)	0.7
Caspofungin	13 (39%)	5 (20%)	3 (8.3%)	5 (21%)	0.020

Continuous variables are described with median and interquartile range and compared with bilateral Wilcoxon test. Fisher's test was used to compare frequencies, except for CMV serology frequencies. GVHD, graft-versus-host disease; CR, complete remission; MTX, methotrexate; MMF, mycophenolate mofetil; N/A: not available.

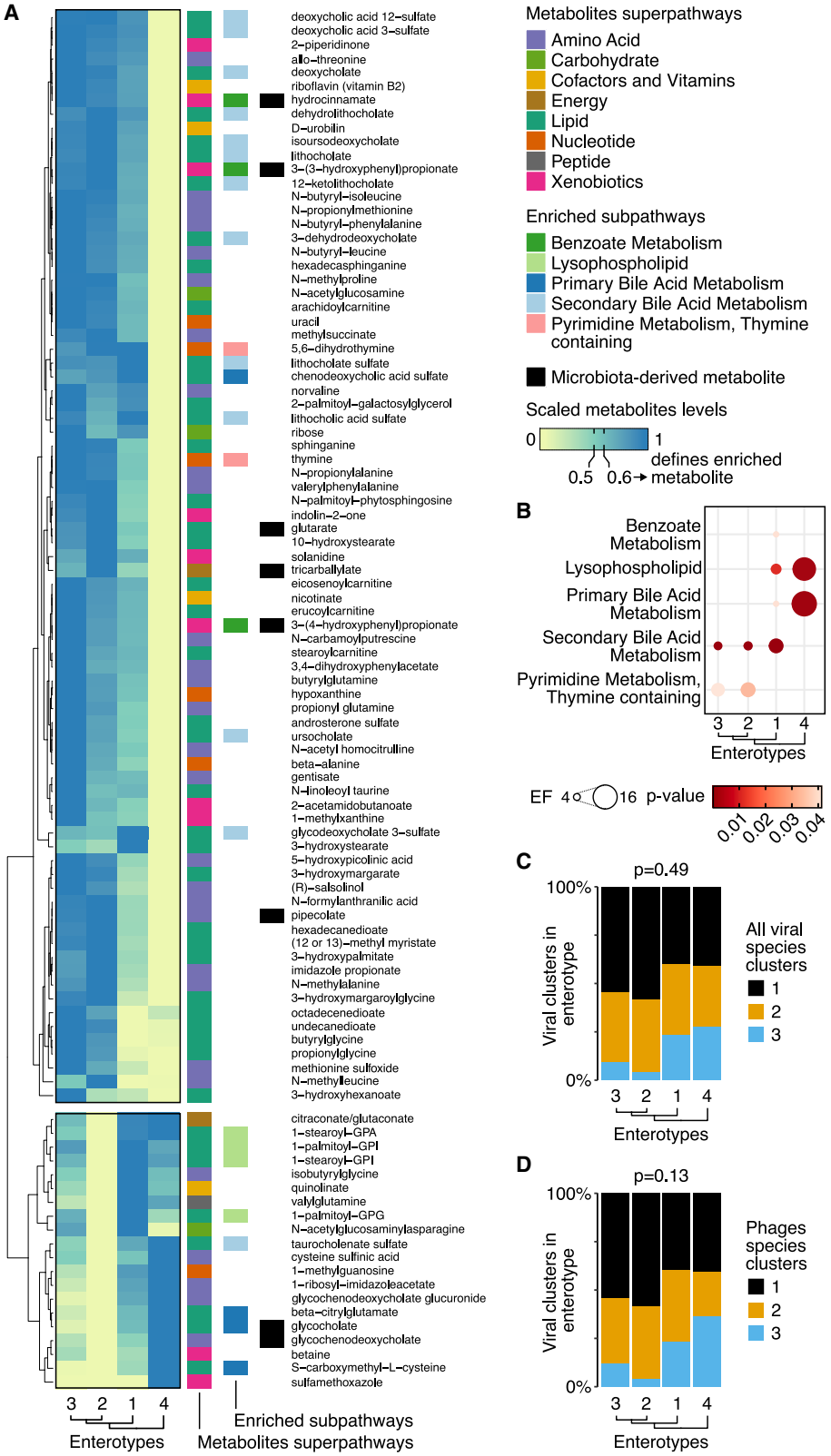

(legend on next page)

other enterotypes, notably enterotype 3, did not reveal a specific pattern (Figures S2D–S2F).

To highlight which bacterial phylotypes or taxa drove metabolic profiles among enterotypes and whether their individual abundance may be associated with gut virome composition, we studied their specific correlations. This led to the identification of 270 statistically significant correlations (Data S5). Louvain clustering was applied to a correlation network to highlight multi-omic modules of highly correlated phylotypes, metabolites, and viral species (Data S6). Summarizing the metabolites associated with bacterial taxa in terms of enriched metabolic pathways revealed that secondary bile acid enrichment was shared by *B. uniformis* (module 11), *E. aerogenes*, and *Prevotella sp. DJF_RP53* (module 1). Sterol pathway enrichment was shared by *Clostridium sp.* (module 10) and *F. prausnitzii* (module 5). Other enriched pathways were specific to modules (Figures 5A and S7A).

Among the 13 modules, module 2 (driven by *Fusobacterium necrophorum*) was associated with 18 viral species, including 14 (78%) bacteriophages. When studying bacteriophages according to their genus, only *Pepyhexaviruses* were commonly associated with phylotypes related to *Prevotella sp*. *DJF_RP53* and *E. aerogenes*. Correlations with unclassified *Siphoviridae* were shared by phylotypes related to *Bacteroides sp.* DJF-B097, *E. faecalis* and *F. necrophorum* (Figure S7B). Among the eukaryotic host viruses, a species of *picobirnaviruses*, *Otarine picobirnavirus*, was associated with a phylotype related to *F. prausnitzii* (module 5).

Considering treatment arm and hematological response status, modules that included the three phylotypes associated with relapse and azithromycin were characterized by statistically significant metabolic pathway enrichments and viral species that were exclusive to these taxa (Figure 5B). *Bacteroides sp*. *DJF_B097*, the phylotype that decreased with azithromycin, was associated with lysophospholipid and phospholipid metabolism. This might be related to azithromycin interactions with cell membrane phospholipids.[29–31] *Prevotella sp*. *DJF_RP53* was associated with pentose metabolism and *B. fragilis* with branched-chain amino acid (BCAA) metabolism pathways (Figure 5C). Regarding viruses, among the six significant species correlated with bacterial phylotypes, five (83%) were bacteriophages. Each genus was specifically correlated with one phylotype (Figure 5D).

Enterotypes and relapse-associated bacterial taxa are correlated to plasma metabolite levels and peripheral blood T cell subsets

Gut microbiota were shown to influence systemic T cell effector function through metabolite biosynthesis.[32–34] To explore how gut microbiota may influence circulating T cells and antitumor immune response, we relied on a multi-omics approach using plasma metabolite and mass cytometry data from our previous work (Figure S8A).[28] We identified 144 plasma metabolites associated with enterotypes. Metabolites associated with enterotypes 2 and 3 were mainly xenobiotic, while those associated with enterotypes 1 and 4 were lipids and amino acids metabolites. In addition, enterotypes 2 and 3 were associated with more microbiota-derived metabolites (n = 15) than enterotypes 1 and 4 (n = 3) (Figure 6A). Subpathway enrichment profiles were comparable for enterotypes 2 and 3, while enterotypes 1 and 4 exhibited specific enriched subpathways (Figure 6B).

Enterotypes were also associated with the frequency of peripheral blood T cell subsets. Enterotypes 2 and 3 were associated with clusters expressing molecules associated with T cell activation or cytotoxic activity, including 2B4, KLRG1, and Granzyme B. Mucosal associated invariant T cells (MAITs) subsets were also associated with enterotype 2. Enterotype 4 was associated with TIGIT+ T cells and Eomes+T-bet+ subsets, while enterotype 1 was associated with co-inhibitory molecules expression, including ICOS, TIGIT, PD-1, and CTLA-4 and also with TOX expression in CD4+ Th1 cells (Figure 6C). This suggested that both relapse-related enterotypes 1 and 4 were associated with exhausted T cells in peripheral blood. At the level of bacterial phylotypes, inter-omic correlations can be explored in the Data S7.

Finally, we unveiled a significant association between *B. fragilis*, the taxon associated with a higher risk of relapse, and exhausted T cells co-expressing TIGIT, PD-1, and TOX in central memory CD4+ Th1 and Th2 cells and CD8+ cells. Instead, the phylotype associated with a lower risk of relapse, *Bacteroides sp*. *DJF_B097*, was associated with KLRG1+2B4+-activated effector memory CD4+ Th0 cells and TIGIT+ central memory CD4+ Th1 cells (Figure 6D).

Overall, these results uncover specific associations between enterotypes, bacterial taxa (or phylotypes), and systemic metabolomic profiles that may influence antitumor T cell responses and relapse risk after allo-HSCT.

DISCUSSION

Early administration of azithromycin after allo-HSCT unexpectedly increased the risk of hematological malignancy relapses in a prospective randomized phase III clinical trial.[11] By using unsupervised and targeted approaches, we revealed the impact of azithromycin treatment on gut microbiota that contributed to relapse. In the context of post-transplantation relapses, we uncovered specific correlations between bacteria, bacteriophages species, metabolic pathways, and circulating immune cells.

Figure 4. Correlations between enterotypes and metabolite levels and viruses' frequency after allogeneic hematopoietic stem cell transplantation

(A) Heatmap showing the metabolites that are significantly associated with enterotypes. Metabolite levels are scaled, and 0.6 on the scale level defines enrichment. On the right, tile colors depict metabolite superpathways of all metabolites and those belonging to statistically significant enriched subpathways. The Kruskal-Wallis test was performed and p value adjusted for multiple comparisons with false discovery rate method. Metabolites identified as microbiota-derived in human metabolome database (https://hmdb.ca) are depicted.

(B) Dot plot summarizing enrichment factors (EFs) and p values of enriched subpathways from differentially detected metabolites levels. Enrichment factors were computed using the over-representation method and p value using the hypergeometric test.

(C and D) Stacked bar plots depicting the frequencies of samples from one enterotype that belong to a cluster of viruses. p values were computed with Fisher's exact test.

See also Figure S6 and Data S1, S2, S3, and S4.

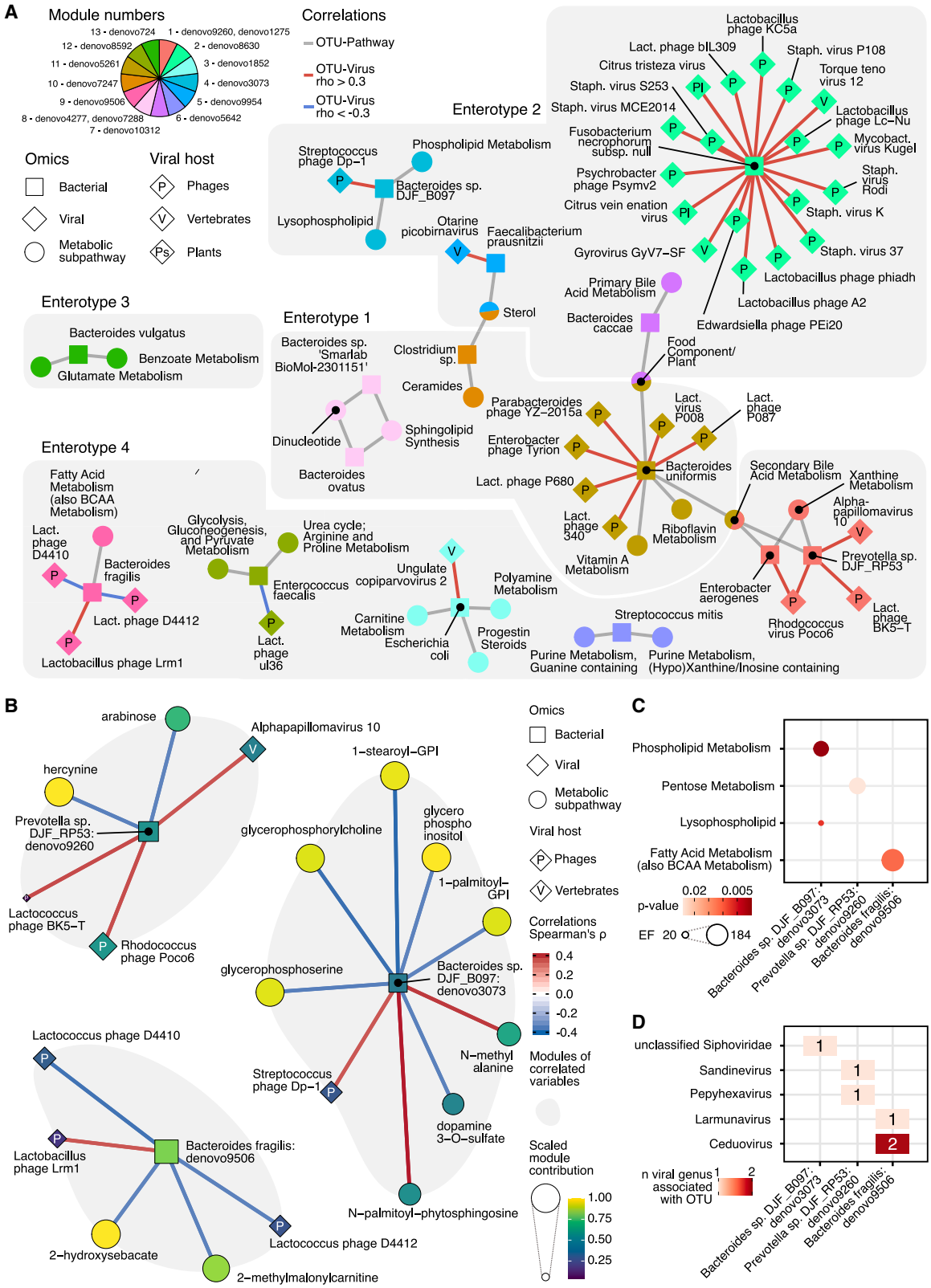

Figure 5. Gut microbiota multi-omics networks associated with azithromycin intake and relapse

(A) Summarized correlation network illustrating subpathways and viral species associated with top enterotype-driving taxa. For visualization purposes, phylotypes are described with the corresponding species names. The network with individual metabolites is available in Data S1.

(legend continued on next page)

We described four enterotypes mainly characterized by *Clostridium sp.*, *B. vulgatus*, *E. faecalis*, *E. aerogenes*, *B. fragilis*, *F. prausnitzii*, and *B. caccae*. This approach has never been reported in this context because previous reports describe gut microbiota in terms of genus[15,17,18,35,36] or a specific species of a genus[37] or clusters of related OTUs.[21] Unlike healthy donors, enterotypes were not persistent across time in this population of heavily treated patients.[38] While the trajectories of enterotypes were heterogeneous, a change of enterotype during the procedure was associated with a lower relapse rate. Diseases and treatments received by patients may explain the differences between reported enterotypes in healthy humans and those from our cohort.[39] Consistent with the results of the MetaCardis cohort, two enterotypes were driven by *Bacteroides*. The enterotype enriched in *B. fragilis* was associated with lower bacterial richness, suggesting dysbiosis.[40]

Consistent with previous reports on allo-HSCT gut microbiota, samples were collected during the allo-HSCT procedure and alpha diversity decreased with time.[15,16,20] The lowest diversity was observed in enterotype 4 (*E. faecalis* and *E. aerogenes*) and the highest with enterotype 2 (*F. prausnitzii*, *B. vulgatus*, and *F. necrophorum*). This is consistent with previous studies that reported lower diversity with *Enterococcus* dominations[41] and higher diversity with *F. prausnitzii*.[42]

Enterotypes were associated with 99 metabolites. Enterotype 4, associated with the lowest diversity, was associated with lower secondary bile acids. Biosynthesis of secondary bile acids from primary bile acids requires bile salt hydroxylases (BSHs).[34] BSHs are expressed by *Bacteroides*, especially *B. vulgatus*,[34,43] which was lower in enterotype 4 compared with other enterotypes. Enterotype 1 was associated with a higher frequency of samples from azithromycin-treated patients. This enterotype was enriched with metabolites from the lysophospholipid pathway. This may be related to the azithromycin impact on membrane phospholipids.[31] Viral species or clusters of viral species were not associated with enterotypes. Other groups have already studied the impact of azithromycin intake on gut microbiota composition and identified consistent impact on bacterial species. More generally, discrepancies on the impact on gut microbiota in mice suggest that microbiota studies based on animal model need to be translated to human.[44–51]

By studying metabolite levels and viruses' frequencies with the top driving bacterial taxa of enterotypes, we identified 13 modules of correlated variables. Strikingly, specific correlations between metabolic pathways, bacteriophages species, and phylotypes were identified. *Picobirnaviridae* were previously reported to be associated with acute gut GVHD.[24] Here, *Otarine picobirnavirus* was positively correlated with *F. prausnitzii* and was classified as a virus of eukaryotic cells. However, as recently described, *Picobirnaviruses* may now be reconsidered as bacteriophages.[52]

Enterotypes were associated with antimicrobial intake. Enterotype 4, enriched in *Enterococcus*, was associated with metronidazole intake, consistent with a previous description of association between antibiotics and *Enterococcus*.[17] The azithromycin group of treatment, type of donor, hematopoietic stem cell (HSC) source and GVHD prophylaxis were associated with enterotypes. Enterotypes were also associated with hematological malignancy outcome, but not with acute GVHD or cGVHD. Belonging to enterotype 2 (*F. prausnitzii*, *B. vulgatus*, and *F. necrophorum*) was associated with complete remission.

Some strains of *F. prausnitzii* were reported to promote local regulatory cells in inflammatory bowel diseases.[42,53] However, in the context of cancers, it is also associated with immune checkpoint inhibitor responses[54] and the inhibition of colorectal cancer cells growth.[55]

Subsequently, we aimed to characterize specific differences of gut microbiota from patients treated with azithromycin or a placebo and from those who relapsed or remained in complete remission. Among the overlapping phylotypes associated with azithromycin, placebo, relapse, and complete remission samples, *Bacteroides sp. DJF_B097* and *Prevotella sp. DJF_RP53* were higher in placebo samples and were associated with complete remission. *B. fragilis* was higher in azithromycin samples and was significantly associated with a higher risk of relapse. This higher risk of relapse with *B. fragilis* was found in both unsupervised multivariate analyses and in supervised methods. A longitudinal study of the three phylotypes' relative abundance revealed that their frequency curves from azithromycin intake overlay relapse patients' curves, while the frequency curves of the placebo group overlay patients in complete remission. *B. fragilis* may dampen antitumor responses by promoting regulatory pathways, as observed in inflammatory bowel diseases in germ-free mice.[56] To date, little is known about the impact of the latter two bacterial taxa on cancer survival and immune responses to tumor cells.

Metabolic pathways enriched with phylotypes associated with relapse or remission were (1) phospholipids and lysophospholipid metabolites in patients with lower *Bacteroides sp. DJF_B097*, which may be explained by the impact of azithromycin on these metabolites,[31] (2) pentose metabolism for *Prevotella sp. DJF_RP53*, and (3) lower BCAA in patients with higher *B. fragilis*, which may be explained by their importance for galactosylceramide biosynthesis.[57]

We revealed specific associations between bacterial taxa and bacteriophages species and genus. Among the taxa associated with relapse, (1) one *Siphoviridae* was associated with *Bacteroides sp. DJF_B097*, (2) one *Sandinevirus* and one *Pepyhexavirus* were associated with *Prevotella sp. DJF_RP53*, and (3) one *Larmunavirus* and two *Ceduovirus* were associated with *B. fragilis*. Bacteriophages are known to impact gut

(B) Correlation network of phylotype frequencies with viral species frequencies and metabolites levels. Modules were identified with the Louvain clustering algorithm. Contribution was computed with principal-component analysis, using variable contribution for the first component.
(C) Dot plot showing enriched metabolite pathways according to phylotypes. Enrichment was calculated with the over-representation method and p value with the hypergeometric test.
(D) Tile plot depicting the number of bacteriophage species from a same viral genus correlated with phylotypes.
Staph, *Staphylococcus*; Lact, *Lactococcus*; Mycobact, *Mycobacterium*.
See also Figure S7 and Data S5 and S6.

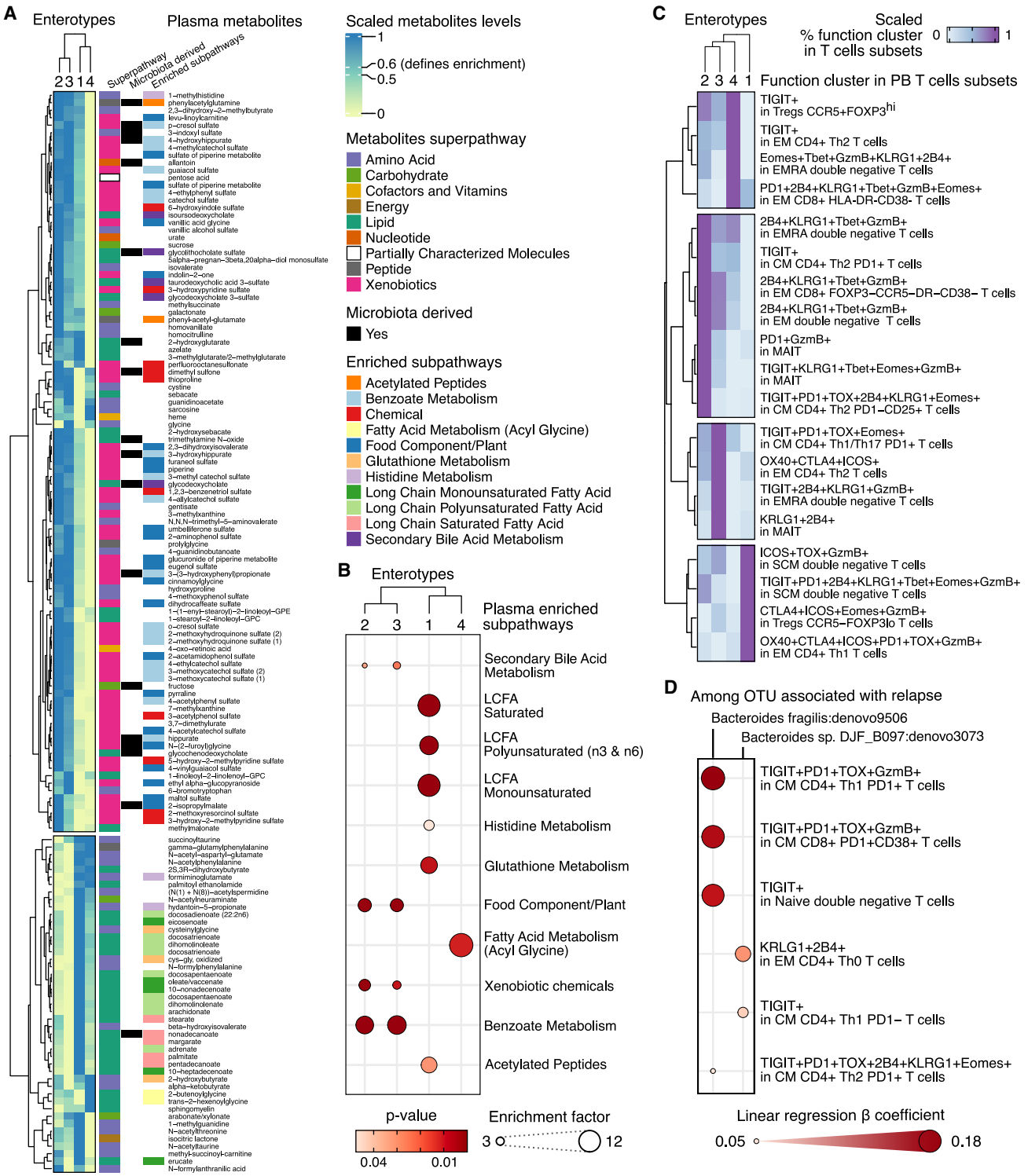

Figure 6. Gut microbiota are associated with plasma metabolites and T cell states

(A) Heatmap showing plasma metabolites significantly associated with enterotypes. Metabolites levels are scaled, and 0.6 on the scale level defines enrichment. On the right, tile colors depict metabolite superpathways of all metabolites and those belonging to a statistically significant enriched subpathway. Metabolites identified as microbiota-derived in the human metabolome database (https://hmdb.ca) are depicted. The Kruskal-Wallis test was performed and p value adjusted for multiple comparisons with false discovery rate method.

(B) Dot plot summarizing the enrichment factors (EFs) and p values of enriched subpathways from differentially detected metabolite levels. Enrichment factors were computed using the over-representation method and p value using the hypergeometric test.

(legend continued on next page)

microbiome composition.[25] They may also impact host metabolism through their interactions with bacterial bile acid metabolism pathways.[58]

Interactions between bacteriophages and bacteria observed in this study might be specific to allo-HSCT because diseases drive bacteriophage and bacteria interactions.[59] Bacteriophages were demonstrated to modify gut microbiome composition and change the course of inflammatory diseases[60–62]; however, the impact of bacteriophages on gut microbiota following allo-HSCT remains to be explored. Conversely, enterotypes were not associated with viral species, but this may be consistent with the specificity of one viral species to bacteria that enterotypes may not encompass.

We recently described that allo-HSCT patients treated with azithromycin exhibited a higher frequency of Th2 and exhausted T cells in samples collected at a median time of 84 days after transplantation.[28] In mice, early-life exposure to azithromycin-perturbed gut microbiota was associated with higher Th2 subsets following allergen exposure.[47] Because thymopoiesis occurs within the 6 months following allo-HSCT,[63] early changes in the microbiota of patients treated with azithromycin may have skewed T cells toward Th2 subsets in naive T cells that encountered allo-antigen. Although we showed a direct effect of azithromycin on T cells *in vitro*, gut microbiota changes may have accentuated the inhibition of antitumor response. T cells expressing co-inhibitory molecules are associated with post-transplant relapse.[64–66] Here, we identified specific correlations between enterotypes, bacterial taxa, and T cell functions. Notably, *B. fragilis* was associated with higher frequency of exhausted T cell profiles, characterized by TIGIT, PD-1, and TOX expression.

Gut microbiota were reported to be associated with 58% of plasma metabolites variance in healthy subjects.[67] Our study reinforces this finding by showing that highly diverse enterotypes 2 and 3 were associated with higher xenobiotic and known microbiota-derived metabolites, while the less-diverse enterotypes 1 and 4 were associated with lipids and amino acid metabolites. Overall, our findings broaden the evidence of gut microbiota's impact on systemic immunity through metabolite processing.[32–34]

The present study aimed to identify biological variables associated with azithromycin or placebo intake and to evaluate their contribution to relapse. Confusion bias cannot be ruled out because of the influence of numerous clinical characteristics on patient outcomes. Nevertheless, included patients and samples were comparable in terms of potential confounding factors, and multivariate analysis revealed that enterotype 2 was independently associated with relapse.

To conclude, studying human fecal samples following allo-HSCT enabled us to identify the complex interplay between gut bacteriome, virome, and metabolic pathways associated with azithromycin intake, which participated in subsequent relapse. Several studies report interactions between gut microbiota and gut virome, notably, bacteriophages' influence on gut microbiota.[25,68,69] Targeted phage therapy against bacterial species involved in inflammatory bowel disease was shown to suppress gut inflammation.[70] Results of our study may provide background to study targeted phage therapy against bacterial species associated with hematological malignancy relapse.

STAR★METHODS

Detailed methods are provided in the online version of this paper and include the following:

- KEY RESOURCES TABLE
- RESOURCE AVAILABILITY
  - Lead contact
  - Materials availability
  - Data and code availability
- EXPERIMENTAL MODEL AND STUDY PARTICIPANT DETAILS
  - Cohort
- METHOD DETAILS
  - Bacteriome
  - Virome
  - Fecal metabolomics
  - Plasma metabolites and T cell subsets
- QUANTIFICATION AND STATISTICAL ANALYSIS
  - Data and statistical analyses

SUPPLEMENTAL INFORMATION

Supplemental information can be found online at https://doi.org/10.1016/j.chom.2023.06.009.

ACKNOWLEDGMENTS

This work was supported by Leucémie Espoir, SOS Oxygène, La Laurène, and EGMOS association. N.V. received financial support from Cancerologie du Centre (CANCEN) and from ITMO Cancer of Aviesan on funds administered by Inserm (allocation number ASC20047HSA). We are grateful to the Genotoul sequencing facility (Get-PlaGe) for amplicons sequencing and the INRAE MIGALE Bioinformatics Facility (MIGALE, INRAE, 2020. Migale Bioinformatics Facility, https://doi.org/10.15454/1.5572390655343293E12), for providing computing and storage resources.

(C) Heatmap describing T cell-state subsets associated with enterotypes. Here, percentage of state cluster among phenotypical subsets are studied. The Kruskal-Wallis test was performed and p value adjusted for multiple comparisons with false discovery rate method. Only a mean frequency of cluster above 0.5% were kept.

(D) Dot plot indicating statistically significant association between relapse-associated taxa and T cell subsets. Here, linear regression models were evaluated. Only state clusters that comprised at least 1% of the phenotypical T cell subsets were kept for the analyses. T cell subsets were defined as the dependent variable of the equation. Only significant adjusted p values for false discovery rate beta coefficients are shown. *Prevotella sp*. *DJF_RP53* is not shown because it was not associated with T cell states.

PB, peripheral blood; Tregs, T regulatory cells; EM, effector memory; EMRA, effector memory CD45RA+; CM, central memory; SCM, stem cell memory; Non-conv, non-conventional; MAITs, mucosal associated invariant T cells.

See also Data S7.

AUTHOR CONTRIBUTIONS

Conceptualization, A.B. and D.M.; methodology, D.M., P.L., J.L.G., and N.V.; formal analysis, N.V.; generation of figures, N.V. and D.M.; investigation, N.V., M.S., J.M.-V., L.B., S.M.-D., S.C., and B.I.; resources, N.V., M.S., S.T., R.P.d.L., A.B., J.L.G., P.L., and D.M.; data curation, N.V., D.M., and L.B., writing – original draft, N.V. and D.M.; writing – review & editing, G.S., A.B., M.S., J.L.G., P.L., and D.M.; visualization, N.V. and D.M.; supervision, D.M. and P.L.; project administration, A.B. and D.M.; funding acquisition, G.S., A.B., and D.M.

DECLARATION OF INTERESTS

G.S. and R.P.d.L. received a research grant from Alexion Pharmaceuticals. R.P.d.L. received a research grant from Novartis and Pfizer. G.S. received fees from Pharmacyclics LLC, Novartis, Incyte, Alexion, Amgen, and Pfizer. D.M. received fees from Novartis, Incyte, Jazz Pharmaceuticals, and CSL Behring. N.V., J.L.G., P.L., and D.M. have a related patent registered under the reference EP22306850.3.

Received: May 15, 2023
Revised: May 23, 2023
Accepted: June 19, 2023
Published: July 17, 2023

REFERENCES

1. Copelan, E.A. (2006). Hematopoietic stem-cell transplantation. N. Engl. J. Med. *354*, 1813–1826. https://doi.org/10.1056/NEJMra052638.
2. Horowitz, M., Schreiber, H., Elder, A., Heidenreich, O., Vormoor, J., Toffalori, C., Vago, L., and Kröger, N. (2018). Epidemiology and biology of relapse after stem cell transplantation. Bone Marrow Transplant. *53*, 1379–1389. https://doi.org/10.1038/s41409-018-0171-z.
3. Blazar, B.R., Hill, G.R., and Murphy, W.J. (2020). Dissecting the biology of allogeneic HSCT to enhance the GvT effect whilst minimizing GvHD. Nat. Rev. Clin. Oncol. *17*, 475–492. https://doi.org/10.1038/s41571-020-0356-4.
4. Horowitz, M.M., Gale, R.P., Sondel, P.M., Kolb, H.-J., Rimm, A.A., Ringden, O., Rozman, C., and Speck, B. (1990). Graft-versus-leukemia reactions after bone marrow transplantation. Blood *8*.
5. Schmid, C., Labopin, M., Nagler, A., Bornhäuser, M., Finke, J., Fassas, A., Volin, L., Gürman, G., Maertens, J., Bordigoni, P., et al. (2007). Donor lymphocyte infusion in the treatment of first hematological relapse after allogeneic stem-cell transplantation in adults with acute myeloid leukemia: a retrospective risk factors analysis and comparison with other strategies by the EBMT acute leukemia working party. J. Clin. Oncol. *25*, 4938–4945. https://doi.org/10.1200/JCO.2007.11.6053.
6. Cho, B.S., Lee, S.E., Song, H.H., Lee, J.H., Yahng, S.A., Eom, K.S., Kim, Y.J., Kim, H.J., Lee, S., Min, C.K., et al. (2012). Graft-versus-tumor effect according to type of graft-versus-host disease defined by National Institutes of Health consensus criteria and associated outcomes. Biol. Blood Marrow Transplant. *18*, 1136–1143. https://doi.org/10.1016/j.bbmt.2012.01.010.
7. Zeiser, R., and Blazar, B.R. (2017). Acute graft-versus-host disease—biologic process, prevention, and therapy. N. Engl. J. Med. *377*, 2167–2179. https://doi.org/10.1056/NEJMra1609337.
8. Bergeron, A., Chevret, S., Peffault de Latour, R., Chagnon, K., de Margerie-Mellon, C., Rivière, F., Robin, M., Mani, J., Lorillon, G., Socié, G., et al. (2018). Noninfectious lung complications after allogeneic haematopoietic stem cell transplantation. Eur. Respir. J. *51*, 1702617. https://doi.org/10.1183/13993003.02617-2017.
9. Barker, A.F., Bergeron, A., Rom, W.N., and Hertz, M.I. (2014). Obliterative bronchiolitis. N. Engl. J. Med. *370*, 1820–1828. https://doi.org/10.1056/NEJMra1204664.
10. Vos, R., Vanaudenaerde, B.M., Verleden, S.E., De Vleeschauwer, S.I., Willems-Widyastuti, A., Van Raemdonck, D.E., Schoonis, A., Nawrot, T.S., Dupont, L.J., and Verleden, G.M. (2011). A randomised controlled trial of azithromycin to prevent chronic rejection after lung transplantation. Eur. Respir. J. *37*, 164–172. https://doi.org/10.1183/09031936.00068310.
11. Bergeron, A., Chevret, S., Granata, A., Chevallier, P., Vincent, L., Huynh, A., Tabrizi, R., Labussiere-Wallet, H., Bernard, M., Chantepie, S., et al. (2017). Effect of azithromycin on airflow decline–free survival after allogeneic hematopoietic stem cell transplant: the ALLOZITHRO randomized clinical trial. JAMA *318*, 557–566. https://doi.org/10.1001/jama.2017.9938.
12. U.S. Food and Drug Administration (2018). FDA warns about increased risk of cancer relapse with long-term use of azithromycin (Zithromax, Zmax) antibiotic after donor stem cell transplant. https://www.fda.gov/drugs/drug-safety-and-availability/fda-warns-about-increased-risk-cancer-relapse-long-term-use-azithromycin-zithromax-zmax-antibiotic.
13. Shono, Y., and van den Brink, M.R.M. (2018). Gut microbiota injury in allogeneic haematopoietic stem cell transplantation. Nat. Rev. Cancer *18*, 283–295. https://doi.org/10.1038/nrc.2018.10.
14. Jenq, R.R., Ubeda, C., Taur, Y., Menezes, C.C., Khanin, R., Dudakov, J.A., Liu, C., West, M.L., Singer, N.V., Equinda, M.J., et al. (2012). Regulation of intestinal inflammation by microbiota following allogeneic bone marrow transplantation. J. Exp. Med. *209*, 903–911. https://doi.org/10.1084/jem.20112408.
15. Peled, J.U., Gomes, A.L.C., Devlin, S.M., Littmann, E.R., Taur, Y., Sung, A.D., Weber, D., Hashimoto, D., Slingerland, A.E., Slingerland, J.B., et al. (2020). Microbiota as predictor of mortality in allogeneic hematopoietic-cell transplantation. N. Engl. J. Med. *382*, 822–834. https://doi.org/10.1056/NEJMoa1900623.
16. Shono, Y., Docampo, M.D., Peled, J.U., Perobelli, S.M., Velardi, E., Tsai, J.J., Slingerland, A.E., Smith, O.M., Young, L.F., Gupta, J., et al. (2016). Increased GVHD-related mortality with broad-spectrum antibiotic use after allogeneic hematopoietic stem cell transplantation in human patients and mice. Sci. Transl. Med. *8*, 339ra71. https://doi.org/10.1126/scitranslmed.aaf2311.
17. Taur, Y., Xavier, J.B., LiPuma, L., Ubeda, C., Goldberg, J., Gobourne, A., Lee, Y.J., Dubin, K.A., Socci, N.D., Viale, A., et al. (2012). Intestinal domination and the risk of bacteremia in patients undergoing allogeneic hematopoietic stem cell transplantation. Clin. Infect. Dis. *55*, 905–914. https://doi.org/10.1093/cid/cis580.
18. Weber, D., Jenq, R.R., Peled, J.U., Taur, Y., Hiergeist, A., Koestler, J., Dettmer, K., Weber, M., Wolff, D., Hahn, J., et al. (2017). Microbiota disruption induced by early use of broad-spectrum antibiotics is an independent risk factor of outcome after allogeneic stem cell transplantation. Biol. Blood Marrow Transplant. *23*, 845–852. https://doi.org/10.1016/j.bbmt.2017.02.006.
19. Jenq, R.R., Taur, Y., Devlin, S.M., Ponce, D.M., Goldberg, J.D., Ahr, K.F., Littmann, E.R., Ling, L., Gobourne, A.C., Miller, L.C., et al. (2015). Intestinal Blautia is associated with reduced death from graft-versus-host disease. Biol. Blood Marrow Transplant. *21*, 1373–1383. https://doi.org/10.1016/j.bbmt.2015.04.016.
20. Taur, Y., Jenq, R.R., Perales, M.A., Littmann, E.R., Morjaria, S., Ling, L., Gobourne, A., Viale, A., Dahi, P.B., et al. (2014). The effects of intestinal tract bacterial diversity on mortality following allogeneic hematopoietic stem cell transplantation. Blood *124*, 1174–1182. https://doi.org/10.1182/blood-2014-02-554725.
21. Peled, J.U., Devlin, S.M., Staffas, A., Lumish, M., Khanin, R., Littmann, E.R., Ling, L., Kosuri, S., Maloy, M., Slingerland, J.B., et al. (2017). Intestinal microbiota and relapse after hematopoietic-cell transplantation. J. Clin. Oncol. *35*, 1650–1659. https://doi.org/10.1200/JCO.2016.70.3348.
22. Postler, T.S., and Ghosh, S. (2017). Understanding the holobiont: how microbial metabolites affect human health and shape the immune system. Cell Metab. *26*, 110–130. https://doi.org/10.1016/j.cmet.2017.05.008.
23. Yang, J.H., Bhargava, P., McCloskey, D., Mao, N., Palsson, B.O., and Collins, J.J. (2017). Antibiotic-induced changes to the host metabolic environment inhibit drug efficacy and alter immune function. Cell Host Microbe *22*, 757–765.e3. https://doi.org/10.1016/j.chom.2017.10.020.

24. Legoff, J., Resche-Rigon, M., Bouquet, J., Robin, M., Naccache, S.N., Mercier-Delarue, S., Federman, S., Samayoa, E., Rousseau, C., Piron, P., et al. (2017). The eukaryotic gut virome in hematopoietic stem cell transplantation: new clues in enteric graft-versus-host disease. Nat. Med. *23*, 1080–1085. https://doi.org/10.1038/nm.4380.

25. Hsu, B.B., Gibson, T.E., Yeliseyev, V., Liu, Q., Lyon, L., Bry, L., Silver, P.A., and Gerber, G.K. (2019). Dynamic modulation of the gut microbiota and metabolome by bacteriophages in a mouse model. Cell Host Microbe *25*, 803–814.e5. https://doi.org/10.1016/j.chom.2019.05.001.

26. Zuppi, M., Hendrickson, H.L., O'Sullivan, J.M., and Vatanen, T. (2021). Phages in the gut ecosystem. Front. Cell. Infect. Microbiol. *11*, 822562. https://doi.org/10.3389/fcimb.2021.822562.

27. Legoff, J., Michonneau, D., and Socie, G. (2020). The virome in hematology—stem cell transplantation and beyond. Semin. Hematol. *57*, 19–25. https://doi.org/10.1053/j.seminhematol.2020.05.001.

28. Vallet, N., Le Grand, S., Bondeelle, L., Hoareau, B., Corneau, A., Bouteiller, D., Tournier, S., Derivry, L., Bohineust, A., Tourret, M., et al. (2022). Azithromycin promotes relapse by disrupting immune and metabolic networks after allogeneic stem cell transplantation. Blood *140*, 2500–2513. https://doi.org/10.1182/blood.2022016926.

29. Montenez, J.P., Van Bambeke, F., Piret, J., Brasseur, R., Tulkens, P.M., and Mingeot-Leclercq, M.P. (1999). Interactions of macrolide antibiotics (erythromycin a, roxithromycin, erythromycylamine [dirithromycin], and azithromycin) with phospholipids: computer-aided conformational analysis and studies on acellular and cell culture models. Toxicol. Appl. Pharmacol. *156*, 129–140. https://doi.org/10.1006/taap.1999.8632.

30. Munić, V., Banjanac, M., Koštrun, S., Nujić, K., Bosnar, M., Marjanović, N., Ralić, J., Matijašić, M., Hlevnjak, M., and Eraković Haber, V.E. (2011). Intensity of macrolide anti-inflammatory activity in J774A.1 cells positively correlates with cellular accumulation and phospholipidosis. Pharmacol. Res. *64*, 298–307. https://doi.org/10.1016/j.phrs.2011.03.011.

31. Van Bambeke, F., Montenez, J.P., Piret, J., Tulkens, P.M., Courtoy, P.J., and Mingeot-Leclercq, M.P. (1996). Interaction of the macrolide azithromycin with phospholipids. I. Inhibition of lysosomal phospholipase A1 activity. Eur. J. Pharmacol. *314*, 203–214. https://doi.org/10.1016/S0014-2999(96)00552-3.

32. Hang, S., Paik, D., Yao, L., Kim, E., Trinath, J., Lu, J., Ha, S., Nelson, B.N., Kelly, S.P., Wu, L., et al. (2019). Bile acid metabolites control TH17 and Treg cell differentiation. Nature *576*, 143–148. https://doi.org/10.1038/s41586-019-1785-z.

33. Mazmanian, S.K., Liu, C.H., Tzianabos, A.O., and Kasper, D.L. (2005). An immunomodulatory molecule of symbiotic bacteria directs maturation of the host immune system. Cell *122*, 107–118. https://doi.org/10.1016/j.cell.2005.05.007.

34. Cai, J., Sun, L., and Gonzalez, F.J. (2022). Gut microbiota-derived bile acids in intestinal immunity, inflammation, and tumorigenesis. Cell Host Microbe *30*, 289–300. https://doi.org/10.1016/j.chom.2022.02.004.

35. Holler, E., Butzhammer, P., Schmid, K., Hundsrucker, C., Koestler, J., Peter, K., Zhu, W., Sporrer, D., Hehlgans, T., Kreutz, M., et al. (2014). Metagenomic analysis of the stool microbiome in patients receiving allogeneic stem cell transplantation: loss of diversity is associated with use of systemic antibiotics and more pronounced in gastrointestinal graft-versus-host disease. Biol. Blood Marrow Transplant. *20*, 640–645. https://doi.org/10.1016/j.bbmt.2014.01.030.

36. Kusakabe, S., Fukushima, K., Maeda, T., Motooka, D., Nakamura, S., Fujita, J., Yokota, T., Shibayama, H., Oritani, K., and Kanakura, Y. (2020). Pre- and post-serial metagenomic analysis of gut microbiota as a prognostic factor in patients undergoing haematopoietic stem cell transplantation. Br. J. Haematol. *188*, 438–449. https://doi.org/10.1111/bjh.16205.

37. Stein-Thoeringer, C.K., Nichols, K.B., Lazrak, A., Docampo, M.D., Slingerland, A.E., Slingerland, J.B., Clurman, A.G., Armijo, G., Gomes, A.L.C., Shono, Y., et al. (2019). Lactose drives *Enterococcus* expansion to promote graft-versus-host disease. Science *366*, 1143–1149. https://doi.org/10.1126/science.aax3760.

38. Cheng, M., and Ning, K. (2019). Stereotypes about enterotype: the old and new ideas. Genomics Proteomics Bioinformatics *17*, 4–12. https://doi.org/10.1016/j.gpb.2018.02.004.

39. Arumugam, M., Raes, J., Pelletier, E., Le Paslier, D., Yamada, T., Mende, D.R., Fernandes, G.R., Tap, J., Bruls, T., Batto, J.M., et al. (2011). Enterotypes of the human gut microbiome. Nature *473*, 174–180. https://doi.org/10.1038/nature09944.

40. Vieira-Silva, S., Falony, G., Belda, E., Nielsen, T., Aron-Wisnewsky, J., Chakaroun, R., Forslund, S.K., Assmann, K., Valles-Colomer, M., Nguyen, T.T.D., et al. (2020). Statin therapy is associated with lower prevalence of gut microbiota dysbiosis. Nature *581*, 310–315. https://doi.org/10.1038/s41586-020-2269-x.

41. Messina, J.A., Tan, C.Y., Ren, Y., Hill, L., Bush, A., Lew, M., Andermann, T., Peled, J.U., Gomes, A., van den Brink, M.R.M., et al. (2021). *Enterococcus* intestinal domination is associated with increased mortality in the acute leukemia chemotherapy population. Clin. Infect. Dis. https://doi.org/10.1093/cid/ciab1043.

42. Sokol, H., Pigneur, B., Watterlot, L., Lakhdari, O., Bermúdez-Humarán, L.G., Gratadoux, J.J., Blugeon, S., Bridonneau, C., Furet, J.P., Corthier, G., et al. (2008). *Faecalibacterium prausnitzii* is an anti-inflammatory commensal bacterium identified by gut microbiota analysis of Crohn disease patients. Proc. Natl. Acad. Sci. USA *105*, 16731–16736. https://doi.org/10.1073/pnas.0804812105.

43. Yao, L., Seaton, S.C., Ndousse-Fetter, S., Adhikari, A.A., DiBenedetto, N., Mina, A.I., Banks, A.S., Bry, L., and Devlin, A.S. (2018). A selective gut bacterial bile salt hydrolase alters host metabolism. eLife *7*, e37182. https://doi.org/10.7554/eLife.37182.

44. Park, H.K., Choi, Y., Lee, D.H., Kim, S., Lee, J.M., Choi, S.W., Lee, H.R., Rho, M., and Park, H.S. (2020). Altered gut microbiota by azithromycin attenuates airway inflammation in allergic asthma. J. Allergy Clin. Immunol. *145*, 1466–1469.e8. https://doi.org/10.1016/j.jaci.2020.01.044.

45. Zhao, H., Zhou, J., Lu, H., Xi, A., Luo, M., Wang, K., Lv, H., Wang, H., Wang, P., Miao, J., et al. (2022). Azithromycin pretreatment exacerbates atopic dermatitis in trimellitic anhydride-induced model mice accompanied by correlated changes in the gut microbiota and serum cytokines. Int. Immunopharmacol. *102*, 108388. https://doi.org/10.1016/j.intimp.2021.108388.

46. Yin, J., M, P., Wang, S., Liao, S.X., Peng, X., He, Y., Chen, Y.R., Shen, H.F., Su, J., Chen, Y., et al. (2015). Different dynamic patterns of β-lactams, quinolones, glycopeptides and macrolides on mouse gut microbial diversity. PLoS One *10*, e0126712. https://doi.org/10.1371/journal.pone.0126712.

47. Borbet, T.C., Pawline, M.B., Zhang, X., Wipperman, M.F., Reuter, S., Maher, T., Li, J., Iizumi, T., Gao, Z., Daniele, M., et al. (2022). Influence of the early-life gut microbiota on the immune responses to an inhaled allergen. Mucosal Immunol. *15*, 1000–1011. https://doi.org/10.1038/s41385-022-00544-5.

48. Doan, T., Arzika, A.M., Ray, K.J., Cotter, S.Y., Kim, J., Maliki, R., Zhong, L., Zhou, Z., Porco, T.C., Vanderschelden, B., et al. (2017). Gut microbial diversity in antibiotic-naive children after systemic antibiotic exposure: a randomized controlled trial. Clin. Infect. Dis. *64*, 1147–1153. https://doi.org/10.1093/cid/cix141.

49. Wei, S., Mortensen, M.S., Stokholm, J., Brejnrod, A.D., Thorsen, J., Rasmussen, M.A., Trivedi, U., Bisgaard, H., and Sørensen, S.J. (2018). Short- and long-term impacts of azithromycin treatment on the gut microbiota in children: a double-blind, randomized, placebo-controlled trial. EBioMedicine *38*, 265–272. https://doi.org/10.1016/j.ebiom.2018.11.035.

50. Anthony, W.E., Wang, B., Sukhum, K.V., D'Souza, A.W., Hink, T., Cass, C., Seiler, S., Reske, K.A., Coon, C., Dubberke, E.R., et al. (2022). Acute and persistent effects of commonly used antibiotics on the gut microbiome and resistome in healthy adults. Cell Rep. *39*, 110649. https://doi.org/10.1016/j.celrep.2022.110649.

51. Pickering, H., Hart, J.D., Burr, S., Stabler, R., Maleta, K., Kalua, K., Bailey, R.L., and Holland, M.J. (2022). Impact of azithromycin mass drug administration on the antibiotic-resistant gut microbiome in children: a

randomized, controlled trial. Gut Pathog. *14*, 5. https://doi.org/10.1186/s13099-021-00478-6.

52. Neri, U., Wolf, Y.I., Roux, S., Camargo, A.P., Lee, B., Kazlauskas, D., Chen, I.M., Ivanova, N., Zeigler Allen, L., Paez-Espino, D., et al. (2022). Expansion of the global RNA virome reveals diverse clades of bacteriophages. Cell *185*, 4023–4037.e18. https://doi.org/10.1016/j.cell.2022.08.023.
53. Touch, S., Godefroy, E., Rolhion, N., Danne, C., Oeuvray, C., Straube, M., Galbert, C., Brot, L., Alonso Salgueiro, I., Chadi, S., et al. (2022). Human CD4+CD8α+ Tregs induced by Faecalibacterium prausnitzii protect against intestinal inflammation. JCI Insight *7*, e154722. https://doi.org/10.1172/jci.insight.154722.
54. Miller, P.L., and Carson, T.L. (2020). Mechanisms and microbial influences on CTLA-4 and PD-1-based immunotherapy in the treatment of cancer: a narrative review. Gut Pathog. *12*, 43. https://doi.org/10.1186/s13099-020-00381-6.
55. Dikeocha, I.J., Al-Kabsi, A.M., Chiu, H.T., and Alshawsh, M.A. (2022). Faecalibacterium prausnitzii ameliorates colorectal tumorigenesis and suppresses proliferation of HCT116 colorectal cancer cells. Biomedicines *10*, 1128. https://doi.org/10.3390/biomedicines10051128.
56. Troy, E.B. (2010). Beneficial effects of Bacteroides fragilis polysaccharides on the immune system. Front. Biosci. *15*, 25–34.
57. Oh, S.F., Praveena, T., Song, H., Yoo, J.S., Jung, D.J., Erturk-Hasdemir, D., Hwang, Y.S., Lee, C.C., Le Nours, J., Kim, H., et al. (2021). Host immunomodulatory lipids created by symbionts from dietary amino acids. Nature *600*, 302–307. https://doi.org/10.1038/s41586-021-04083-0.
58. Campbell, D.E., Ly, L.K., Ridlon, J.M., Hsiao, A., Whitaker, R.J., and Degnan, P.H. (2020). Infection with Bacteroides phage BV01 alters the host transcriptome and bile acid metabolism in a common human gut microbe. Cell Rep. *32*, 108142. https://doi.org/10.1016/j.celrep.2020.108142.
59. De Sordi, L., Lourenço, M., and Debarbieux, L. (2019). The battle within: interactions of bacteriophages and bacteria in the gastrointestinal tract. Cell Host Microbe *25*, 210–218. https://doi.org/10.1016/j.chom.2019.01.018.
60. Duan, Y., Llorente, C., Lang, S., Brandl, K., Chu, H., Jiang, L., White, R.C., Clarke, T.H., Nguyen, K., Torralba, M., et al. (2019). Bacteriophage targeting of gut bacterium attenuates alcoholic liver disease. Nature *575*, 505–511. https://doi.org/10.1038/s41586-019-1742-x.
61. Fujimoto, K., Kimura, Y., Shimohigoshi, M., Satoh, T., Sato, S., Tremmel, G., Uematsu, M., Kawaguchi, Y., Usui, Y., Nakano, Y., et al. (2020). Metagenome data on intestinal phage-bacteria associations Aids the development of phage therapy against pathobionts. Cell Host Microbe *28*, 380–389.e9. https://doi.org/10.1016/j.chom.2020.06.005.
62. Galtier, M., De Sordi, L., Sivignon, A., de Vallée, A., Maura, D., Neut, C., Rahmouni, O., Wannerberger, K., Darfeuille-Michaud, A., Desreumaux, P., et al. (2017). Bacteriophages targeting adherent invasive *Escherichia coli* strains as a promising new treatment for Crohn's disease. J. Crohns. Colitis *11*, 840–847. https://doi.org/10.1093/ecco-jcc/jjw224.
63. Dumont-Girard, F., Roux, E., van Lier, R.A., Hale, G., Helg, C., Chapuis, B., Starobinski, M., and Roosnek, E. (1998). Reconstitution of the T-cell compartment after bone marrow transplantation: restoration of the repertoire by thymic emigrants. Blood *92*, 4464–4471. https://doi.org/10.1182/blood.V92.11.4464.
64. Gournay, V., Vallet, N., Peux, V., Vera, K., Bordenave, J., Lambert, M., Corneau, A., Michonneau, D., Peffault de Latour, R., Caillat-Zucman, S., et al. (2022). Immune landscape after allo-HSCT: TIGIT and CD161-expressing CD4 T cells are associated with subsequent leukemia relapse. Blood *140*, 1305–1321. https://doi.org/10.1182/blood.2022015522.
65. Noviello, M., Manfredi, F., Ruggiero, E., Perini, T., Oliveira, G., Cortesi, F., De Simone, P., Toffalori, C., Gambacorta, V., Greco, R., et al. (2019). Bone marrow central memory and memory stem T-cell exhaustion in AML patients relapsing after HSCT. Nat. Commun. *10*, 1065. https://doi.org/10.1038/s41467-019-08871-1.
66. Hutten, T.J.A., Norde, W.J., Woestenenk, R., Wang, R.C., Maas, F., Kester, M., Falkenburg, J.H.F., Berglund, S., Luznik, L., Jansen, J.H., et al. (2018). Increased coexpression of PD-1, TIGIT, and KLRG-1 on tumor-reactive CD8+ T cells during relapse after allogeneic stem cell transplantation. Biol. Blood Marrow Transplant. *24*, 666–677. https://doi.org/10.1016/j.bbmt.2017.11.027.
67. Dekkers, K.F., Sayols-Baixeras, S., Baldanzi, G., Nowak, C., Hammar, U., Nguyen, D., Varotsis, G., Brunkwall, L., Nielsen, N., Eklund, A.C., et al. (2022). An online atlas of human plasma metabolite signatures of gut microbiome composition. Nat. Commun. *13*, 5370. https://doi.org/10.1038/s41467-022-33050-0.
68. Shkoporov, A.N., Clooney, A.G., Sutton, T.D.S., Ryan, F.J., Daly, K.M., Nolan, J.A., McDonnell, S.A., Khokhlova, E.V., Draper, L.A., Forde, A., et al. (2019). The human gut virome is highly diverse, stable, and individual specific. Cell Host Microbe *26*, 527–541.e5. https://doi.org/10.1016/j.chom.2019.09.009.
69. Wahida, A., Tang, F., and Barr, J.J. (2021). Rethinking phage-bacteria-eukaryotic relationships and their influence on human health. Cell Host Microbe *29*, 681–688. https://doi.org/10.1016/j.chom.2021.02.007.
70. Federici, S., Kredo-Russo, S., Valdés-Mas, R., Kviatcovsky, D., Weinstock, E., Matiuhin, Y., Silberberg, Y., Atarashi, K., Furuichi, M., Oka, A., et al. (2022). Targeted suppression of human IBD-associated gut microbiota commensals by phage consortia for treatment of intestinal inflammation. Cell *185*, 2879–2898.e24. https://doi.org/10.1016/j.cell.2022.07.003.
71. R Core Team (2022). R: A language and environment for statistical computing. R Foundation for Statistical Computing, Vienna, Austria. URL https://www.R-project.org/.
72. Calle, M.L., and Susin, A. (2022). Identification of dynamic microbial signatures in longitudinal studies. Preprint at bioRxiv. https://doi.org/10.1101/2022.04.25.489415.
73. Pedersen, T. (2022). ggraph: An Implementation of Grammar of Graphics for Graphs and Networks. https://ggraph.data-imaginist.com, https://github.com/thomasp85/ggraph.
74. Lê, S., Josse, J., and Husson, F. (2008). FactoMineR: an R package for multivariate analysis. J. Stat. Soft. *25*. https://doi.org/10.18637/jss.v025.i01.
75. Gerds, T.A., and Kattan, M.W. (2021). Medical Risk Prediction Models: With Ties to Machine Learning, 1st ed. (Chapman and Hall/CRC). https://doi.org/10.1201/9781138384484.
76. Kassambara, A., and Mundt, F. (2020). Extract and visualize the results of multivariate data analyses. R Package, version 1.0.7. https://CRAN.R-project.org/package=factoextra.
77. McMurdie, P.J., and Holmes, S. (2013). phyloseq: An R package for reproducible interactive analysis and graphics of microbiome census data. PLoS ONE *8*, e61217.
78. Oksanen, J., Simpson, G.L., Blanchet, G., and Kindt, R. (2022). vegan: community ecology package. R package version 2.6-2. https://CRAN.R-project.org/package=vegan.
79. Cybis G.B., Valk M., and Lopes S.R.C. (2018). Clustering and classification problems in genetics through U-statistics. https://doi.org/10.1080/00949655.2017.1374387.
80. Caporaso, J.G., Kuczynski, J., Stombaugh, J., Bittinger, K., Bushman, F.D., Costello, E.K., Fierer, N., Peña, A.G., Goodrich, J.K., Gordon, J.I., et al. (2010). QIIME allows analysis of high-throughput community sequencing data. Nat. Methods *7*, 335–336. https://doi.org/10.1038/nmeth.f.303.
81. Wang, Q., Garrity, G.M., Tiedje, J.M., and Cole, J.R. (2007). Naive Bayesian Classifier for Rapid Assignment of rRNA Sequences into the New Bacterial Taxonomy. Appl Environ Microbiol *73*, 5261–5267.
82. Bolger, A.M., Lohse, M., and Usadel, B. (2014). Trimmomatic: a flexible trimmer for Illumina sequence data. Bioinformatics *30*, 2114–2120. https://doi.org/10.1093/bioinformatics/btu170.
83. Gregg, F., and Eder, D. (2022). Dedupe. GitHub. https://github.com/dedupeio/dedupe.

84. Wood, D.E., Lu, J., and Langmead, B. (2019). Improved metagenomic analysis with Kraken 2. Genome Biol. *20*, 257. https://doi.org/10.1186/s13059-019-1891-0.

85. Altschul, S.F., Gish, W., Miller, W., Myers, E.W., and Lipman, D.J. (1990). Basic local alignment search tool. J. Mol. Biol. *215*, 403–410.

86. Vallet, N., Michonneau, D., and Tournier, S. (2022). Toward practical transparent verifiable and long-term reproducible research using Guix. Sci. Data *9*, 597. https://doi.org/10.1038/s41597-022-01720-9.

87. Qin, J., Li, R., Raes, J., Arumugam, M., Burgdorf, K.S., Manichanh, C., Nielsen, T., Pons, N., Levenez, F., Yamada, T., et al. (2010). A human gut microbial gene catalogue established by metagenomic sequencing. Nature *464*, 59–65. https://doi.org/10.1038/nature08821.

88. Cole, J.R., Wang, Q., Cardenas, E., Fish, J., Chai, B., Farris, R.J., Kulam-Syed-Mohideen, A.S., McGarrell, D.M., Marsh, T., Garrity, G.M., et al. (2009). The Ribosomal Database Project: improved alignments and new tools for rRNA analysis. Nucleic Acids Res. *37*, D141–D145. https://doi.org/10.1093/nar/gkn879.

89. Miller, S., Naccache, S.N., Samayoa, E., Messacar, K., Arevalo, S., Federman, S., Stryke, D., Pham, E., Fung, B., Bolosky, W.J., et al. (2019). Laboratory validation of a clinical metagenomic sequencing assay for pathogen detection in cerebrospinal fluid. Genome Res. *29*, 831–842. https://doi.org/10.1101/gr.238170.118.

90. Michonneau, D., Latis, E., Curis, E., Dubouchet, L., Ramamoorthy, S., Ingram, B., de Latour, R.P., Robin, M., de Fontbrune, F.S., Chevret, S., et al. (2019). Metabolomics analysis of human acute graft-versus-host disease reveals changes in host and microbiota-derived metabolites. Nat. Commun. *10*, 5695. https://doi.org/10.1038/s41467-019-13498-3.

91. Wishart, D.S., Tzur, D., Knox, C., Eisner, R., Guo, A.C., Young, N., Cheng, D., Jewell, K., Arndt, D., Sawhney, S., et al. (2007). HMDB: the human metabolome database. Nucleic Acids Res. *35*, D521–D526. https://doi.org/10.1093/nar/gkl923.

92. Kim, S., Chen, J., Cheng, T., Gindulyte, A., He, J., He, S., Li, Q., Shoemaker, B.A., Thiessen, P.A., Yu, B., et al. (2021). PubChem in 2021: new data content and improved web interfaces. Nucleic Acids Res. *49*, D1388–D1395. https://doi.org/10.1093/nar/gkaa971.

STAR★METHODS

KEY RESOURCES TABLE

REAGENT or RESOURCE	SOURCE	IDENTIFIER
Antibodies		
Anti-human CD5-143Nd (clone: UCHT2)	Standard BioTools	(Standard BioTools Cat# 3143007B, RRID:AB_2921325)
Anti-human CD11a-142Nd (clone: HI111)	Standard BioTools	(Standard BioTools Cat# 3142006B, RRID:AB_2877095)
Anti-human CD95/Fas-152Sm (clone: DX2)	Standard BioTools	(Standard BioTools Cat# 3152017B, RRID:AB_2920762)
Anti-human CD197/CCR7-159Tb (clone: G043H7)	Standard BioTools	Cat# 3159003A, RRID:**AB_2938859**
Anti-human CD195/CCR5-156Gd (clone: NP-6G4)	Standard BioTools	Cat# 3156015A, **RRID:AB_2938860**
Anti-human CD127/IL-7Rα-165Ho (clone: A019D5)	Standard BioTools	(Standard BioTools Cat# 3165008B, RRID:AB_2868401)
Anti-human CD16-209Bi (clone: 3G8)	Standard BioTools	(Standard BioTools Cat# 3209002B, RRID:AB_2756431)
Anti-human CD25/IL-2R-169Tm (clone: 2A3)	Standard BioTools	Cat# 3169003B, **RRID:AB_2938861**
Anti-human CD27-167Er (clone: L128)	Standard BioTools	(Standard BioTools Cat# 3167006B, RRID:AB_2811093)
Anti-human IgD-146Nd (clone: IA6-2)	Standard BioTools	(Standard BioTools Cat# 3146005B, RRID:AB_2811082)
Anti-human KLRG1-168Er (clone: 4C2A07)	Biolegend	(BioLegend Cat# 368602, RRID:AB_2566256)
Anti-human CD45RA-170Er (clone: HI100)	Standard BioTools	Cat# 3170010B, **RRID:AB_2938862**
Anti-human TIGIT-154Sm (clone: MBSA43)	Standard BioTools	(Standard BioTools Cat# 3154016B, RRID:AB_2888926)
Anti-human CD45-89Y (clone: HI30)	Standard BioTools	Cat# 3089003B, **RRID:AB_2938863**
Anti-human CD20-147Sm (clone: 2H7)	Standard BioTools	(Standard BioTools Cat# 3147001B, RRID:AB_2921324)
Anti-human CD161-164Dy (clone: HP-3G10)	Standard BioTools	(Standard BioTools Cat# 3164009B, RRID:AB_2687651)
Anti-human CD183 /CXCR3-163Dy (clone: G025H7)	Standard BioTools	(Standard BioTools Cat# 3163004B, RRID:AB_2810969)
Anti-human CD3-141Pr (clone: UCHT1)	Standard BioTools	Cat# 3141019B, **RRID:AB_2938864**
Anti-human FoxP3-162Dy (clone: 259D/C7)	Standard BioTools	Cat# 3162024A, **RRID:AB_2938865**
Anti-human CD279/PD-1-155Gd (clone: EH12.2H7)	Standard BioTools	(Standard BioTools Cat# 3155009B, RRID:AB_2811087)
Anti-human CD185/CXCR5-171Yb (clone: 51505)	Standard BioTools	Cat# 3171006B, **RRID:AB_2938866**
Anti-human Granzyme B-173Yb (clone: GB11)	Standard BioTools	(Standard BioTools Cat# 3173006B, RRID:AB_2811095)
Anti-human CD24-166Er (clone: ML5)	Standard BioTools	Cat# 3166007B, **RRID:AB_2938867**
Anti-human CD38-144Nd (clone: HIT2)	Standard BioTools	(Standard BioTools Cat# 3144014B, RRID:AB_2687640)
Anti-human TIM-3-153Eu (clone: F38-2E2)	Standard BioTools	Cat# 3153008B, **RRID:AB_2938868**
Anti-human CD134/OX40-150Nd (clone: ACT35)	Standard BioTools	Cat# 3150023B, **RRID:AB_2938869**
Anti-human CD223/LAG-3-175Lu (clone: 11C3C65)	Standard BioTools	(Standard BioTools Cat# 3175033B, RRID:AB_2888932)
Anti-human CD152/CTLA-4-161Dy (clone: 14D3)	Standard BioTools	(Standard BioTools Cat# 3161004B, RRID:AB_2687649)
Anti-human Tbet-160Gd (clone: 4B10)	Standard BioTools	(Standard BioTools Cat# 3160010B, RRID:AB_2810251)

(*Continued on next page*)

Continued

REAGENT or RESOURCE	SOURCE	IDENTIFIER
Anti-human CD137/4-1BB-158Gd (clone: 4B4-1)	Standard BioTools	(Standard BioTools Cat# 3158013B, RRID:AB_2888927)
Anti-human CD56/NCAM-176Yb (clone: NCAM16.2)	Standard BioTools	Cat# 3176008B, **RRID:AB_2938870**
Anti-human IgM-172Yb (clone: MHM-88)	Standard BioTools	(Standard BioTools Cat# 3172004B, RRID:AB_2810858)
Anti-human CD278/ICOS-148Nd (clone: C398.4A)	Standard BioTools	(Standard BioTools Cat# 3148019B, RRID:AB_2756435)
Anti-human CD244/2B4-145Nd (clone: CI.7)	Biolegend	(BioLegend Cat# 329502, RRID:AB_1279194)
Anti-human CD194/CCR4-149Sm (clone: L291H4)	Standard BioTools	Cat# 3149029A, **RRID:AB_2938871**
Anti-human Tox-151Eu (clone: TXRX10)	Thermo Fisher	(Thermo Fisher Scientific Cat# 14-6502-82, RRID:AB_10718252)
Anti-human Eomes-174Yb (clone: 644730)	Thermo Fisher	(Thermo Fisher Scientific Cat# MA5-24291, RRID:AB_2609866)
Anti-human CD14-106Cd (clone: M5E2)	Biolegend	(BioLegend Cat# 301843, RRID:AB_2562813)
Anti-human CD19-110Cd (clone: HIB19)	Biolegend	(BioLegend Cat# 302247, RRID:AB_2562815)
Anti-human CD4-111Cd (clone: SK3)	Biolegend	(BioLegend Cat# 344625, RRID:AB_2563749)
Anti-human CD8-113Cd (clone: SK1)	Biolegend	(BioLegend Cat# 344727, RRID:AB_2563762)
Anti-human HLA-DR-114Cd (clone: L243)	Biolegend	(BioLegend Cat# 307651, RRID:AB_2562826)
Anti-human TCR Vα7-2-116Cd (clone: 3C10)	Biolegend	(BioLegend Cat# 351702, RRID:AB_10900258)
Anti-human CD3-BV785 (clone: OKT3)	Biolegend	(BioLegend Cat# 317330, RRID:AB_2563507)
Anti-human CD4-BV605 (clone: OKT4)	Biolegend	(BioLegend Cat# 317438, RRID:AB_11218995)
Anti-human CD4-BV510 (clone: SK3)	Biolegend	(BioLegend Cat# 344634, RRID:AB_2566017)
Anti-human CD8-APC (clone: SK1)	Biolegend	(BioLegend Cat# 344722, RRID:AB_2075388)
Anti-human Rabbit monoclonal SOCS1 (clone: EPR24290-356)	Abcam	Cat# ab280886, **RRID:AB_2938872**
Anti-human Rabbit IgG monoclonal (clone: EPR25A)	Abcam	(Abcam Cat# ab172730, RRID:AB_2687931)
Anti-rabbit Goat IgG H&L-AF488	Abcam	(Abcam Cat# ab150077, RRID:AB_2630356)
Biological samples		
Feces samples	MICROBIOTE-T3 (IRB 00003835)	Cohort
PBMCs (patients)	Cryostem biobank	Mass cytometry cohort
Plasma samples (patients)	Cryostem biobank	Plasma metabolome cohort
Critical commercial assays		
MoBio Power Fecal DNA isolation kit	MoBio	CAT#12830-50
TURBO DNAse	Invitrogen	CAT#AM2239
Baseline-ZERO DNase	Ambion	Not available
Benzonase® Nuclease	Millipore	CAT#70664-3
RNAse A	Promega	CAT#A7974
NucliSENS easyMAG	Biomerieux	CAT#280140
NEBNext ® Microbiome DNA Enrichment Kit	NEB	CAT#E2612 S/L

(*Continued on next page*)

Continued

REAGENT or RESOURCE	SOURCE	IDENTIFIER
Zymo DNA Clean and Concentrator	Zymo	CAT#D4014
Nextera XT library preparation kit	Illumina	CAT#FC-131-1096
Trio RNA Kit	TECAN	CAT# 401141 V1
MaxPar® X8 antibody labeling 151Eu	Fluidigm	201151A
MaxPar® X8 antibody labeling 174 Yb	Fluidigm	201174A
MaxPar® X8 antibody labeling 145 Nd	Fluidigm	201145A
MaxPar® X8 antibody labeling 168 Er	Fluidigm	201168A
MaxPar® MCP9 antibody labeling 106 Cd	Fluidigm	201106A
MaxPar® MCP9 antibody labeling 110 Cd	Fluidigm	201110A
MaxPar® MCP9 antibody labeling 111 Cd	Fluidigm	201111A
MaxPar® MCP9 antibody labeling 113 Cd	Fluidigm	201113A
MaxPar® MCP9 antibody labeling 114 Cd	Fluidigm	201114A
MaxPar® MCP9 antibody labeling 116 Cd	Fluidigm	201116A
Deposited data		
Metabolomic data	This paper	Metabolight: MTBLS406
Shotgun sequencing	This paper	SRA Bioproject: PRJNA898682
16S RNA	This paper	SRA Bioproject: PRJNA902819
RefSeq	NCBI	https://ftp.ncbi.nlm.nih.gov/genomes/refseq/
Raw mass cytometry data	Vallet et al.[28]	FlowRepository: FR-FCM-Z5ZB
Raw metabolomic data	Vallet et al.[28]	Metabolights: MTBLS406
Processed Mass cytometry data	Software Heritage	https://archive.softwareheritage.org/swh:1:dir:16a829f98f9d8d707343b3b48bc13f5d641998d9
Processed Plasma metabolome data	Software Heritage	https://archive.softwareheritage.org/swh:1:dir:16a829f98f9d8d707343b3b48bc13f5d641998d9
Software and algorithms		
MacOS	Apple	V 11.5.1
Inkscape: Open Source Scalable Vector Graphics Editor	https://inkscape.org/	V 1.2.1
R (see version number in manuscript and Guix, configurations)	R Core Team[71]	https://cran.r-project.org/
R package: coda4microbiome	Calle et al.[72]	https://cran.r-project.org/web/packages/coda4microbiome/index.html
R package: ggraph	Pedersen[73]	https://github.com/thomasp85/ggraph
R package: FactoMineR	Lê et al.[74]	http://factominer.free.fr/
R package: riskRegression	Gerds team[75]	https://github.com/tagteam/riskRegression
R package: factoextra	Kassambara and Mundt[76]	https://CRAN.R-project.org/package=factoextra
R package: phyloseq	McMurdie and Holmes[77]	https://github.com/joey711/phyloseq
R package: vegan	Oksanen et al.[78]	https://CRAN.R-project.org/package=vegan
R package: uclust	Cybis et al.[79]	https://cran.r-project.org/web/packages/uclust/index.html
Quantitative Insights Into Microbial Ecology	Caporaso et al.[80]	http://qiime.org/
RDP classifier	Wang et al.[81]	http://rdp.cme.msu.edu/index.jsp
TRIMMOMATIC	Bolger et al.[82]	http://www.usadellab.org/cms/?page=trimmomatic

(*Continued on next page*)

Continued

REAGENT or RESOURCE	SOURCE	IDENTIFIER
Dedupe	Gregg and Eder[83]	https://github.com/dedupeio/dedupe
Kraken2	Wood et al.[84]	https://ccb.jhu.edu/software/kraken2/
Blastn	Altschul et al.[85]	https://blast.ncbi.nlm.nih.gov/
Source code for analyses	This paper	https://gitlab.com/nivall/azimutfeces
Chemicals, peptides, and recombinant proteins		
PierceTM Universal Nuclease	Thermofisher	88702
Cisplatine Cell-ID	Fluidigm	201064
Mass cytometry staining buffer	Fluidigm	201068
Fc Receptor Blocking Solution	Biolegend	422302
Paraformaldehyde	Electron Microscopy Sciences-	15713
Perm Buffer	eBioscience	00-8333-56
Fixation/permeabilization buffer	eBioscience	00-5523-00
Intercalator-Iridium	Fluidigm	201192B
MaxPar Cell Acquisition Solution	Fluidigm	201241
Oligonucleotides		
Primers V3-V4	Eurofins	N/A

RESOURCE AVAILABILITY

Lead contact

Further information and requests for resources and reagents should be directed to and will be fulfilled by the lead contact, David Michonneau (david.michonneau@aphp.fr)

Materials availability

This study did not generate new unique reagents

Data and code availability

Raw data are available on a public repository: (i) metabolomic, Metabolights: MTBLS406; (ii) bacteriome, Bioproject: PRJNA902819; (iii) virome, Bioproject: PRJNA898682. Source codes, data and CSV files of interim analyses are available on the following Git repositories: https://gitlab.com/nivall/azimutfeces. Git repositories version at submission time are archived on Software Heritage: https://archive.softwareheritage.org/swh:1:dir:9a24ab367cbe9519007f0dd407423fe47def5cfa. Unless otherwise specified, data analyses were computed using R environment. Raw figures were made with the "ggplot2" R package. Computational environment may be reproduced using GNU Guix with the files "manifest.scm" and "channels.scm" in "guixconfig" directory of the git repository.[86] Manuscript figures were created from R outputs and combined with Inkscape (version 1.2.1) on macOS (version 12.5).

EXPERIMENTAL MODEL AND STUDY PARTICIPANT DETAILS

Cohort

This study was conducted with samples from patients included in the multicenter, randomized, double-blind, placebo-controlled phase three superiority trial ALLOZITHRO (NCT01959100).[11] This study was approved by the local ethics committee and Institutional Review Board (CPP Île de France IV, IRB number 00003835, reference number 2013-000499-14). Fecal samples were gathered from the cohort MICROBIOTE-T3 (IRB 00003835, CNIL 104706). Blood samples were retrieved from the CRYOSTEM Consortium (project number CS-1801, IRB Sud-Méditerranée 1, reference AC-2011-1420) and the Commission National Informatique et Liberté for data protection (reference nz70243374i no. 912120). All patients gave written consent for clinical research. No additional clinical procedure was carried out in this non-interventional research study in accordance with the Declaration of Helsinki. Data analyses were performed using a database without patients' identifiers. Patients' characteristics are described in Tables 1 and S1. Feces and blood samples collection times are shown in Figure S8A.

METHOD DETAILS

Bacteriome

Sample processing and 16SrRNA sequencing

Patients' fecal samples were frozen-aliquoted (150 mg), homogenized and lysed using both mechanical (bead beating for 10 minutes) and chemical techniques as previously described,[87] and total DNA was extracted using the MoBio Power Fecal DNA isolation kit

following the manufacturer's recommendations. DNA quality and quantity were evaluated using a spectrophotometer (Nanodrop 1000, Thermoscientific). Sequencing was then performed at GeT-PlaGe platform of the Génopole (Toulouse Midi-Pyrénées, France) using Illumina MiSeq technology targeting the V3-V4 region of the 16SrRNA gene with the following primers: V3fwd-TACGGRAGG CAGCAG and V4rev- TACCAGGGTATCTAAT.

Phylotype identification pipeline

The raw sequences were analyzed using the open source software package Quantitative Insights Into Microbial Ecology (QIIME).[80] After trimming primers and barcodes, the sequences were filtered for quality (minimum length= 300bp, minimum quality threshold=20, chimeras removed) and clustered into phylotypes at a threshold of 97% similarity level (operational taxonomic units; OTUs) using UCLUST. Samples amplified but resulting in less than 500 reads were removed. The most abundant member of each OTU was selected as the representative sequence and assigned to different taxonomic levels using the RDP naïve Bayesian classifier and RDP Seqmatch program.[88] Estimates of the richness and alpha-diversity of phylotypes were calculated using the number of observed OTUs, Shannon and Simpson indices on the rarefied OTU table (n=3,000 reads). An average of 14,677 reads were obtained per sample (ranging from 3,056 to 24,545).

Virome

DNA and RNA virome analysis with shotgun Next Generation Sequencing

Fecal samples (solid phase) were re-suspended and diluted (50%) in phosphate buffered saline (PBS) and then centrifuged at 2500 g for 20 minutes. To enrich for viral particles by reduction of host background, stool supernatant was filtered through a 0.45 μm filter (Corning Costar Spin-X centrifuge tube filters), and an aliquot of 315 μl of filtrate was pre-treated before extraction by incubation with different nucleases: TURBO DNAse (Invitrogen, Carlsbad, CA); Baseline-ZERO DNase (Ambion, Foster City, CA); Benzonase (NEB); RNAse A (Promega) for 30 min, at 37 °C. Total nucleic acids were extracted using NucliSENS easyMAG (Biomerieux) according to the manufacturers' protocol. For the preparation of DNA libraries, 25 μL of extract was used. Depletion of methylated host DNA was performed using NEBNext ® Microbiome DNA Enrichment Kit (NEB) according to the manufacturers' instructions. DNA was then purified using zymo DNA Clean (Zymo) and eluted in 7.5 μL of sterile water. DNA libraries were prepared using Nextera XT library preparation kit (Illumina). For the preparation of RNA libraries, Trio RNA Kit (TECAN) was used according to the manufacturers' instructions. Libraries were sequenced on an Illumina HiSeq X (16 lanes) using 150/150-bp paired-end sequencing.

Species identification pipeline

Raw reads were cleaned using TRIMMOMATIC.[82] Duplicated reads were removed using Dedupe.[83] Taxonomic assignment was carried out using Kraken2, with Viral, Bacterial and Human Refseq databases.[84] Kraken viral assigned reads were verified using Blastn on Refseq viral database. Reads with inconsistent assignment between Kraken and Blast methods were removed. Samples with less than 5.10^6 reads were excluded. Data with less than 0.5 reads per million (RPM) were assimilated to 0. Variables were filtered according to mean RPM in seven negative controls.[89] DNA and RNA reads databases were then merged to obtain a final count database.

Fecal metabolomics

Sample processing

Samples were processed and analyzed by Ultrahigh Performance Liquid Chromatography-Tandem Mass Spectroscopy (UPLC-MS/MS) by Metabolon (Durham, USA). Acquisition, quality control and metabolites identification and quantification were performed as previously described.[90]

Pathway identification

To assign metabolic pathways, the list of identified metabolites was manually compared with Metabolon, Human Metabolome Database[91] and PubChem[92] databases.

Metabolite data preprocessing

Uncharacterized metabolites were excluded from the analyses. Quantification of metabolites was normalized to dry weight of fecal material extracted. Missing values (metabolites below quantification threshold) were imputed with 50% of the minimum value of the corresponding metabolite, and metabolites with more than 50% of missing values were excluded. Regarding drugs-related metabolites, missing values were imputed with 1% of the minimum value and none of the metabolites were excluded. Finally, 925 known metabolites were analyzed (Figure S8B).

Plasma metabolites and T cell subsets

Plasma metabolites and T cell subsets data were reported in a previous work from our group.[28] Briefly, frozen plasma aliquots were processed by Metabolon (Durham, USA). Metabolomics data acquisition using UPLC-MS/MS, quality assurance/quality control, compounds identification and quantification were performed by Metabolon. Considering T cell subsets identification and quantification, thawed peripheral blood mononuclear cells (PBMC) were stained with 43 metal-conjugated antibodies and processed to mass cytometer. FlowSOM clustering on 31 phenotypical antigens identified 55 PBMC subsets. Among these clusters, 30 T cell subsets (CD3+ cells) were then clustered with FlowSOM in 25 state clusters according to 14 states antigens, including: granzyme B, Eomes, Tbet, KLRG1, 2B4, Thymocyte Selection Associated High Mobility Group Box (TOX), PD-1, TIGIT, ICOS, CTLA-4, OX40, 4-1BB, LAG-3, TIM-3. This allowed us to identify activated, resting and exhausted subsets among phenotypical subsets of T cells.

All data were fetched from the repository associated with our previous work[28]: available on Gitlab, https://gitlab.com/nivall/azimut-blood/ and preserved for the long-term on Software Heritage, https://archive.softwareheritage.org/swh:1:dir:16a829f98f9d8d707343b3b48bc13f5d641998d9.

QUANTIFICATION AND STATISTICAL ANALYSIS

Data and statistical analyses

Enterotype definition

A "vegan" package was used to compute dissimilarity matrix with Bray-Curtis and UniFrac methods for bacterial and viral data, respectively.[78] Dimension reduction of the dissimilarity matrix was done with principal coordinate analysis (PCoA). Sample clustering was performed with hierarchical k-means with the package "factoextra"[76]. To identify leading genera and phylotypes in the clustering, we used permutational multivariate analysis of variance (PERMANOVA) with 999 permutations.

Dynamic microbiome signatures

The "coda4microbiome" package was used to identify meta-variables that would recapitulate a dynamic microbiome signature.[72]

Correlation analysis

Using non-parametric Spearman's method, a correlation matrix was computed with every variable from the three omics. To keep the correlation relevant, only those with an absolute rho co-efficient above 0.3 and statistically significant (false discovery rate adjusted p-value < 0.05) were kept. Regarding phylotypes, feces metabolites and viral species correlations, we selected the top 10 enterotype-driving phylotypes (Figure S8C), the 99 metabolites associated with enterotypes and all viral species.

Correspondence analysis

Correspondence analysis was performed with "FactoMineR" package,[74] with all antibiotics used during the allo-HSCT procedure.

Metabolomic analyses

Pathway enrichment was evaluated with an enrichment factor computed with over-representation analysis method. When studying enterotype enriched pathways, significant metabolites were defined with a 0 to 1 normalized value above 0.6. Statistical testing to enrichment was achieved with hypergeometric distribution.[90]

Network analysis

The networks were built from correlation matrices. Each node shows one variable and edges depict significant correlations. In metabolic enriched pathway analyses, edges depict a link between the pathway and the phylotype. For visualization purposes, the Fruchterman-Reingold algorithm was used.

Network modules analysis

Modules were defined after Louvain clustering was applied to build networks. Principal component analysis (PCA) was used to calculate contribution and loadings of each variable into the module. Variables included in one module are included in a PCA. Then, loadings are computed with variables co-ordinates on the first PCA axis. For each sample, we computed the module variables by summing individual variables weighted with the loadings.

Survival analyses

The incidence of relapse was computed with a competing risk model using the Fine and Gray method. The starting point was the day of infused graft (D0), death was considered as a competing risk event and relapse the event. Mean value was applied in cases of multiple samples from one patient.

Statistical tests

A distribution of variables is non-gaussian, bilateral, non-parametric tests were used. To study the association of enterotypes with feces and plasma metabolites, viruses and T cell subsets, a non-parametric Kruskal-Wallis test was used. Frequency comparisons were performed with a chi-squared or Fisher's test. False discovery rate method was used to correct p-value for multiple testing with Benjamini-Hochberg method. Multinomial regression was used to build models to test multivariate association between enterotypes and clinical variables. Linear regression models were built to test multivariate association between modules and clinical variables. To evaluate phylotypes associations with T cell subsets, linear regression was used: mean phylotype frequency association with T cell subsets was evaluated.